IFIC/13-34

Short-range mechanisms of neutrinoless double beta decay at the LHC

J.C. Helo* and S.G. Kovalenko†
Universidad Técnica Federico Santa María, Centro-Científico-Tecnológico de Valparaíso, Casilla 110-V, Valparaíso, Chile

M. Hirsch‡
AHEP Group, Instituto de Física Corpuscular – C.S.I.C./Universitat de València Edificio de Institutos de Paterna, Apartado 22085, E–46071 València, Spain

H. Päs§
Fakultät für Physik, Technische Universität Dortmund, D-44221, Dortmund, Germany

Abstract

Lepton number violation (LNV) mediated by short range operators can manifest itself in both neutrinoless double beta decay ($0\nu\beta\beta$) and in processes with same sign dilepton final states at the LHC. We derive limits from existing LHC data at $\sqrt{s} = 8$ TeV and compare the discovery potential of the forthcoming $\sqrt{s} = 14$ TeV phase of the LHC with the sensitivity of current and future $0\nu\beta\beta$ decay experiments, assuming the short-range part of the $0\nu\beta\beta$ decay amplitude dominates. We focus on the first of two possible topologies triggered by one fermion and two bosons in the intermediate state. In all cases, except for the pure leptoquark mechanism, the LHC will be more sensitive than $0\nu\beta\beta$ decay in the future. In addition, we propose to search for a charge asymmetry in the final state leptons and to use different invariant mass peaks as a possibility to discriminate the various possible mechanisms for LNV signals at the LHC.

Keywords: supersymmetry; neutrino masses and mixing; LHC

*Electronic address: juan.heloherrera@gmail.com
†Electronic address: Sergey.Kovalenko@usm.cl
‡Electronic address: mahirsch@ific.uv.es
§Electronic address: heinrich.paes@uni-dortmund.de

I. INTRODUCTION

Neutrinoless double beta ($0\nu\beta\beta$) is well-known as a sensitive probe for lepton number violating (LNV) extensions of the standard model (SM). Possible contributions to the $0\nu\beta\beta$ decay amplitude beyond the minimal mass mechanism [1] have been discussed in the literature for many models: Left-right (LR) symmetric extensions of the SM [1, 2], R-parity violating supersymmetry, both trilinear $\not{R}_P$ [3, 4] and bilinear $\not{R}_P$ [5, 6], leptoquarks [7], sterile neutrinos [8, 9], composite neutrinos [10], Kaluza-Klein towers of neutrinos in models with extra dimensions [11], colour octet scalars [12] or colour sextet diquarks [13–15]. A recent review of "exotics" in $0\nu\beta\beta$ decay can be found, for example, in [16].

However, an observation of $0\nu\beta\beta$ decay will not easily be interpreted as evidence for any specific model. Several ideas to distinguish different contributions to $0\nu\beta\beta$ decay have been discussed in the literature, among them are: (i) Measure the angular distribution of the outgoing electrons [2, 17]; (ii) Compare rates in $0\nu\beta^+/EC$ decays with $0\nu\beta^-\beta^-$ decays [18] and (iii) compare rates of $0\nu\beta^-\beta^-$ decays in different nuclei [19]. In principle, all these three methods could serve to distinguish the long-range right-handed current term (denoted ϵ^{V+A}_{V+A} in our notation and $\langle\lambda\rangle$ in the notation of [2]) from other contributions. However, distinguishing among all the remaining contributions by measurements from $0\nu\beta\beta$ decay experiments only seems practically impossible, mainly due to the large uncertainties in the nuclear matrix element calculations.

Contributions to the $0\nu\beta\beta$ decay rate can be divided into a long-range [20] and a short-range [21] part. In long-range contributions a light neutrino is exchanged between two point-like vertices, not necessarily SM charged-current vertices. This can lead, in those cases where one of the vertices contains a violation of L by $\Delta L = 2$, to very stringent limits on the new physics scale $\Lambda/(\lambda^{\rm LNV}_{\rm eff}) \gtrsim (100 - 1000)$ TeV. Here, $\lambda^{\rm LNV}_{\rm eff}$ is some effective lepton number violating (LNV) coupling depending in the model under consideration. In the short-range part of the amplitude, on the other hand, all exchanged particles are heavy. [2] $0\nu\beta\beta$ decay in this case behaves as a true effective dimension-9 operator:

$$\mathcal{O}^{0\nu\beta\beta}_{d=9} = \frac{c_9}{\Lambda^5}\bar{u}\bar{u}dd\bar{e}\bar{e}. \tag{1}$$

The general decomposition of $\mathcal{O}^{0\nu\beta\beta}_{d=9}$ has very recently been given in [22]. Using the results of [21] and [22], one finds that current limits on the $0\nu\beta\beta$ decay half-lives for ^{76}Ge [23] and ^{136}Xe [24, 25], both of the order of $T^{0\nu\beta\beta}_{1/2} \gtrsim 10^{25}$ ys, correspond to roughly $\Lambda \gtrsim (1.2 - 3.2) g^{4/5}_{eff}$ TeV, where g_{eff} is some effective coupling (see section IV C) depending on the exact decomposition. Obviously, new physics at such scales should be testable at the LHC.

The prototype example of a short-range contribution which has been discussed both for

[1] Exchange of a Majorana neutrino between two SM charged-current vertices leads to an amplitude $\mathcal{A}^{0\nu\beta\beta} \propto \langle m_\nu\rangle \equiv \sum_i U^2_{ei} m_i$, the so-called mass mechanism.

[2] From the view-point of $0\nu\beta\beta$ decay, heavy means masses greater than (only) a few GeV, since the scale to compare with is the nuclear Fermi scale, $p_F \simeq (100 - 200)$ MeV.

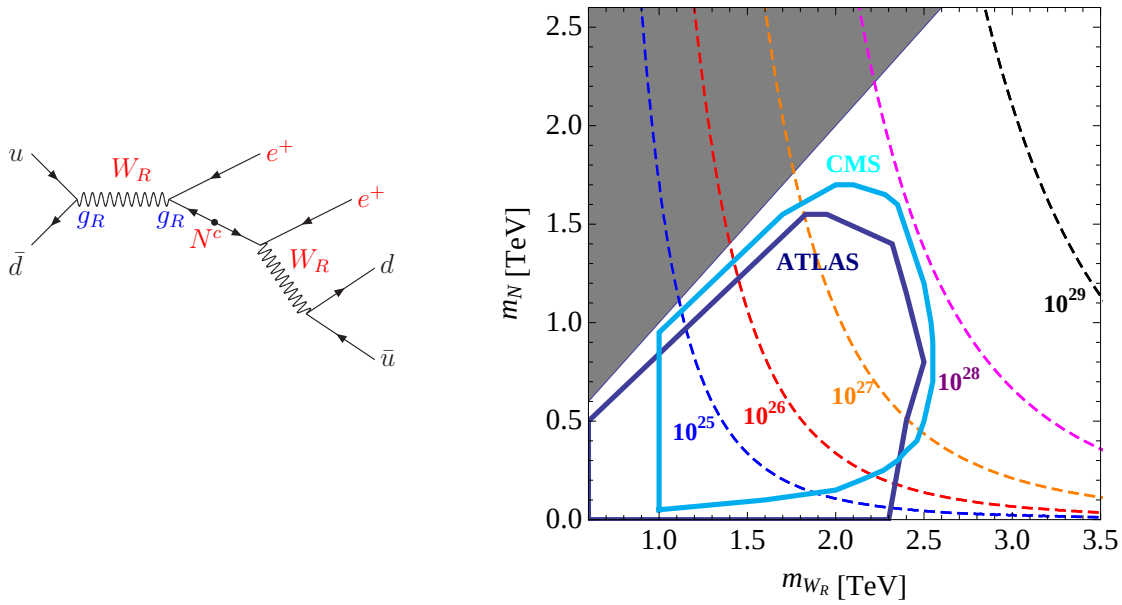

FIG. 1: Example diagram (left) and comparison of sensitivities of the LHC experiments with $0\nu\beta\beta$ decay (right) for a (manifest) left-right symmetric extension of the standard model. Shown are the expected contours for the $0\nu\beta\beta$ decay half-life of ^{76}Ge (contours for ^{136}Xe are very similar) in comparison with the excluded regions from two recent experimental studies by ATLAS [26] and CMS [27] in the plane $m_N - m_{W_R}$, see text.

double beta decay and at the LHC are diagrams mediated by right-handed W-bosons arising in left-right-symmetric extension of the Standard Model [1, 28]. Here, W_R can be produced resonantly on-shell at the LHC and will decay to a right-handed neutrino plus charged lepton, see fig. (1). The right-handed neutrino decays via an off-shell $(W_R)^*$, thus the signal is both, like-sign and opposite sign, dileptons with (at least) two jets and no missing energy [28–31]. Fig. (1) shows a comparison of sensitivities of the LHC experiments with $0\nu\beta\beta$ decay within this framework. Contours show the expected half-lifes for ^{76}Ge $0\nu\beta\beta$ decay using the nuclear matrix elements of [32]. Note that contours for the $0\nu\beta\beta$ decay of ^{136}Xe are very similar. Also shown are the excluded regions from two recent experimental studies by ATLAS [26] and CMS [27]. Both LHC analyses assume that the coupling of the right-handed W boson to fermions has exactly the same strength as the SM W boson coupling to fermions ("manifest left-right symmetry") and the $0\nu\beta\beta$ decay half-lives have therefore been calculated with the same value of the coupling. However, the $0\nu\beta\beta$ decay rate sums over all mass eigenstates m_{N_i}, which couple to electrons, while the LHC experiments assume that m_N appears on-shell in the W_R decay. Thus, this comparison is strictly valid only if (i) only one heavy neutrino appears in the LHC decay chain and (ii) this neutrino couples only to electron pairs (i.e. possible generation mixing is neglected for simplicity here). Note that limits on W_R combining the electron and muon channels at the LHC are slightly more stringent than the ones shown in fig.(1) [27].

We mention in passing that resonant slepton production in R-Parity violating SUSY leads

to the same like-sign dilepton signal [33]. The connection of $\not{R}_P$ SUSY at the LHC with double beta decay has been studied in [34, 35]. Also a variant of the diagram in fig. 1, but with the SM W_L bosons and a heavy sterile neutrino N mixed with the active ones represent a mechanism of $0\nu\beta\beta$ decay, which implications for the LHC have been studied in [36].

In this paper we will generalize this comparison between double beta decay and LHC to the complete list of short-range decompositions ("diagrams") of topology-I (see next section) worked out in [22]. We consider singly charged scalar bosons, leptoquarks and diquarks, as well as the coloured fermions, which appear in the general decomposition of the neutrinoless double beta operator. We mention in passing that a brief summary of our main results has been presented before in a conference [37] and in [38].

The rest of this paper is organized as follows: In section II we briefly review the general decomposition of $\mathcal{O}_{d=9}^{0\nu\beta\beta}$ developed in [22] and make contact with the Lorentz-invariant parametrization of the decay rate worked out in [21]. Section III discusses the production cross sections for different scalars. A numerical analysis, comparing current and future LHC sensitivities with double beta decay, case-by-case for all possible scalar contributions to the $0\nu\beta\beta$ decay rate, is then performed in section IV C. We then turn to the question, whether different models (or decompositions) can actually be distinguished at the LHC, if a positive signal were found in the future. We discuss two types of observables, which allow to do so. First, in section V A we discuss the "charge asymmetry", i.e. the ratio of the number of positron-like to electron-like dilepton (plus jets) events. We then turn to the discussion of invariant mass peaks in V B. A joint analysis of charge asymmetry and invariant mass peaks would allow to identify the dominant contribution to double beta decay. Finally, we close with a short summary of our main results.

II. DECOMPOSITION OF THE $d = 9$ $0\nu\beta\beta$ DECAY OPERATOR

In order to be able to compare the sensitivities of the LHC and $0\nu\beta\beta$ decay experiments input from both particle and nuclear physics is needed. In this section we will briefly recapitulate the main results of two papers [21, 22], which we will use in the later parts of this work. In [22] a general decomposition of the d=9 $0\nu\beta\beta$ decay operator was given. This work allows to identify all possible contributions to $0\nu\beta\beta$ decay from the particle physics point of view. Moreover, it makes contact with the general Lorentz-invariant parametrization of the $0\nu\beta\beta$ deay rate of [20, 21]. These latter papers developed a general formalism and gave numerical values for nuclear matrix elements, which allow to calculate the expected $0\nu\beta\beta$ decay half-lives for any particle physics model.

We start by recalling that there are only two basic topologies which can generate the double beta decay operator at tree-level. These are shown in fig. (2), for brevity we will call them T-I and T-II in the following. While all outer particles in these diagrams are fermions, internal particles can be scalars, fermions or vectors. For topology-I (T-I) all three possible combinations (SFS, SFV and VFV) can lead to models, which give sizeable contributions to $0\nu\beta\beta$ decay. Note that, for T-II one derivative coupling (cases VVV and SVV) or one

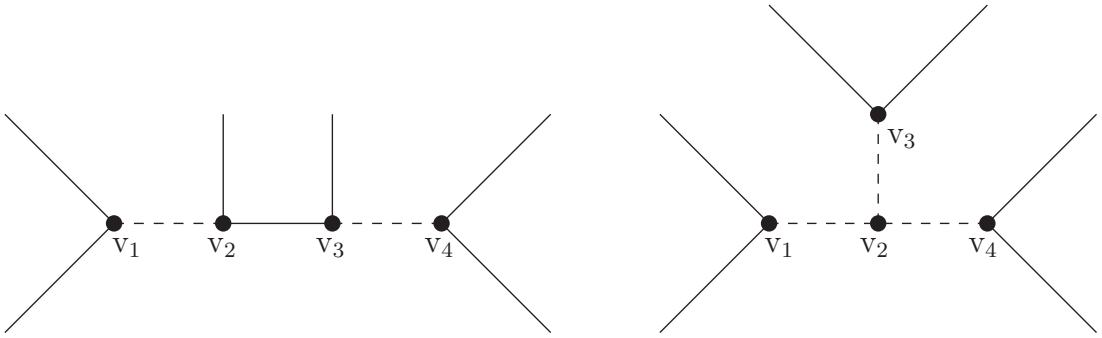

FIG. 2: *The two basic tree-level topologies realizing a $d = 9$ $0\nu\beta\beta$ decay operator. External lines are fermions; internal lines can be fermions (solid), scalars (dashed) or vectors instead of scalars (not shown). For T-I there are in total 3 possibilities classified as: SFS, VFS and VFV.*

dimensionful vertex (cases SSS and VVS) is needed. We plan to deal with T-II, which requires a slightly more complicated analysis, in a future publication [39].

For assigning the fermions to the outer legs in fig. (2) for T-I there exist a total of 18 possibilities. These are listed in table (I), together with the electric charge and possible colour transformation properties of the intermediate state particles. Note that in these tables the chiralities of the fermions are not given, thus the hypercharge of the mediators is not fixed. We will come back to this point below. The table is valid for both, scalars and vectors, although later on we will concentrate on the scalar case. The results for vectors are very similar (apart from some minor numerical factors), so we will only briefly comment on these differences in our numerical analysis.

Table (I) contains six decompositions in which the intermediate state fermion has zero electric charge. All T-I like contributions to $0\nu\beta\beta$ decay, discussed in the literature prior to [22], are variants of these six decompositions. Just to mention two examples, T-I-1-i with vectors coupling to right-handed fermions correspond to the $W_R - N - W_R$ exchange diagram of the left-right symmetric model, discussed briefly in the introduction, while the up-squark diagram of trilinear R-parity breaking supersymmetry [3, 4] is classified as SFS of T-I-4-i with chirality $(\bar{u}_L u_R^c)(\bar{e}_L d_R)(\bar{e}_L d_R)$. The remaining 12 decompositions all require fractionally charged fermions with non-trivial colour transformation properties. They require also the presence of either diquarks or leptoquarks or both.

For most, but not all possibilities listed in table (I) two possibilities for the colour of the intermediate states exist. This is a straight-forward consequence of the SU(3) multiplication rules: $\mathbf{3} \otimes \overline{\mathbf{3}} = \mathbf{1} + \mathbf{8}$ and $\mathbf{3} \otimes \mathbf{3} = \overline{\mathbf{3}}_a + \mathbf{6_s}$. The exception is the case of scalar diquarks, where in all cases except 2-iii-b only the $\mathbf{6_s}$ contributes, since the (scalar) anti-triplet coupling to two identical fermions vanishes [40].

Fig. (3) shows some example diagrams, corresponding to the decompositions (1-i) (diagram a); (2-iii-a) (diagram b); (1-ii) (diagram c) and (3-i) (diagram d). These examples

		Mediator $(Q_{\rm em}, SU(3)_c)$		
#	Decomposition	S or V_ρ	ψ	S' or V'_ρ
1-i	$(\bar{u}d)(\bar{e})(\bar{e})(\bar{u}d)$	$(+1, \mathbf{1} \oplus \mathbf{8})$	$(0, \mathbf{1} \oplus \mathbf{8})$	$(-1, \mathbf{1} \oplus \mathbf{8})$
1-ii-a	$(\bar{u}d)(\bar{u})(d)(\bar{e}\bar{e})$	$(+1, \mathbf{1} \oplus \mathbf{8})$	$(+5/3, \mathbf{3})$	$(+2, \mathbf{1})$
1-ii-b	$(\bar{u}d)(d)(\bar{u})(\bar{e}\bar{e})$	$(+1, \mathbf{1} \oplus \mathbf{8})$	$(+4/3, \overline{\mathbf{3}})$	$(+2, \mathbf{1})$
2-i-a	$(\bar{u}d)(d)(\bar{e})(\bar{u}\bar{e})$	$(+1, \mathbf{1} \oplus \mathbf{8})$	$(+4/3, \overline{\mathbf{3}})$	$(+1/3, \overline{\mathbf{3}})$
2-i-b	$(\bar{u}d)(\bar{e})(d)(\bar{u}\bar{e})$	$(+1, \mathbf{1} \oplus \mathbf{8})$	$(0, \mathbf{1} \oplus \mathbf{8})$	$(+1/3, \overline{\mathbf{3}})$
2-ii-a	$(\bar{u}d)(\bar{u})(\bar{e})(d\bar{e})$	$(+1, \mathbf{1} \oplus \mathbf{8})$	$(+5/3, \mathbf{3})$	$(+2/3, \mathbf{3})$
2-ii-b	$(\bar{u}d)(\bar{e})(\bar{u})(d\bar{e})$	$(+1, \mathbf{1} \oplus \mathbf{8})$	$(0, \mathbf{1} \oplus \mathbf{8})$	$(+2/3, \mathbf{3})$
2-iii-a	$(d\bar{e})(\bar{u})(d)(\bar{u}\bar{e})$	$(-2/3, \overline{\mathbf{3}})$	$(0, \mathbf{1} \oplus \mathbf{8})$	$(+1/3, \overline{\mathbf{3}})$
2-iii-b	$(d\bar{e})(d)(\bar{u})(\bar{u}\bar{e})$	$(-2/3, \overline{\mathbf{3}})$	$(-1/3, \mathbf{3_a} \oplus \overline{\mathbf{6_s}})$	$(+1/3, \overline{\mathbf{3}})$
3-i	$(\bar{u}\bar{u})(\bar{e})(\bar{e})(dd)$	$(+4/3, \overline{\mathbf{3}}_\mathbf{a} \oplus \mathbf{6_s})$	$(+1/3, \overline{\mathbf{3}}_\mathbf{a} \oplus \mathbf{6_s})$	$(-2/3, \overline{\mathbf{3}}_\mathbf{a} \oplus \mathbf{6_s})$
3-ii	$(\bar{u}\bar{u})(d)(d)(\bar{e}\bar{e})$	$(+4/3, \overline{\mathbf{3}}_\mathbf{a} \oplus \mathbf{6_s})$	$(+5/3, \mathbf{3})$	$(+2, \mathbf{1})$
3-iii	$(dd)(\bar{u})(\bar{u})(\bar{e}\bar{e})$	$(+2/3, \mathbf{3_a} \oplus \overline{\mathbf{6}}_\mathbf{s})$	$(+4/3, \overline{\mathbf{3}})$	$(+2, \mathbf{1})$
4-i	$(d\bar{e})(\bar{u})(\bar{u})(d\bar{e})$	$(-2/3, \overline{\mathbf{3}})$	$(0, \mathbf{1} \oplus \mathbf{8})$	$(+2/3, \mathbf{3})$
4-ii-a	$(\bar{u}\bar{u})(d)(\bar{e})(d\bar{e})$	$(+4/3, \overline{\mathbf{3}}_\mathbf{a} \oplus \mathbf{6_s})$	$(+5/3, \mathbf{3})$	$(+2/3, \mathbf{3})$
4-ii-b	$(\bar{u}\bar{u})(\bar{e})(d)(d\bar{e})$	$(+4/3, \overline{\mathbf{3}}_\mathbf{a} \oplus \mathbf{6_s})$	$(+1/3, \overline{\mathbf{3}}_\mathbf{a} \oplus \mathbf{6_s})$	$(+2/3, \mathbf{3})$
5-i	$(\bar{u}\bar{e})(d)(d)(\bar{u}\bar{e})$	$(-1/3, \mathbf{3})$	$(0, \mathbf{1} \oplus \mathbf{8})$	$(+1/3, \overline{\mathbf{3}})$
5-ii-a	$(\bar{u}\bar{e})(\bar{u})(\bar{e})(dd)$	$(-1/3, \mathbf{3})$	$(+1/3, \overline{\mathbf{3}}_\mathbf{a} \oplus \mathbf{6_s})$	$(-2/3, \overline{\mathbf{3}}_\mathbf{a} \oplus \mathbf{6_s})$
5-ii-b	$(\bar{u}\bar{e})(\bar{e})(\bar{u})(dd)$	$(-1/3, \mathbf{3})$	$(-4/3, \mathbf{3})$	$(-2/3, \overline{\mathbf{3}}_\mathbf{a} \oplus \mathbf{6_s})$

TABLE I: *General decomposition of the $d = 9$ operator $\bar{u}\bar{u}dd\bar{e}\bar{e}$ for topology I. The chirality of outer fermions is left unspecified, thus the mediators are given with the charge $Q_{\rm em}$ of electromagnetic $U(1)_{\rm em}$ and that of colour $SU(3)_c$. The symbols S and S' denote scalars, V_ρ and V'_ρ vectors, and ψ a fermion. The table follows the recent paper [22], where more complete tables including chiralities can be found.*

contain at least one example for each of the six different scalars and the four different fermions which appear in table (I). Diagrams for all other decompositions can be straightforwardly derived using the table. Note that, assigning all outer fermions to be right-handed and replacing S_{+1} by a vector corresponds to the diagram for the LR-symmetric model, discussed in the introduction.

In [20, 21] a general Lorentz-invariant description of the $0\nu\beta\beta$ decay rate has been derived. The Lagrangian for the short-range part of the amplitude can be written as [21]

$$\mathcal{L} = \frac{G_F^2}{2} m_p^{-1} \left(\epsilon_1 JJj + \epsilon_2 J^{\mu\nu} J_{\mu\nu} j + \epsilon_3 J^\mu J_\mu j + \epsilon_4 J^\mu J_{\mu\nu} j^\nu + \epsilon_5 J^\mu J j_\mu \right) . \tag{2}$$

Here we omitted the chiral indices for clarity. However, for the case of $\epsilon_3 - \epsilon_5$, where chirality changes play a role in the value of the neutrinoless beta decay rate, the indices need to be kept.

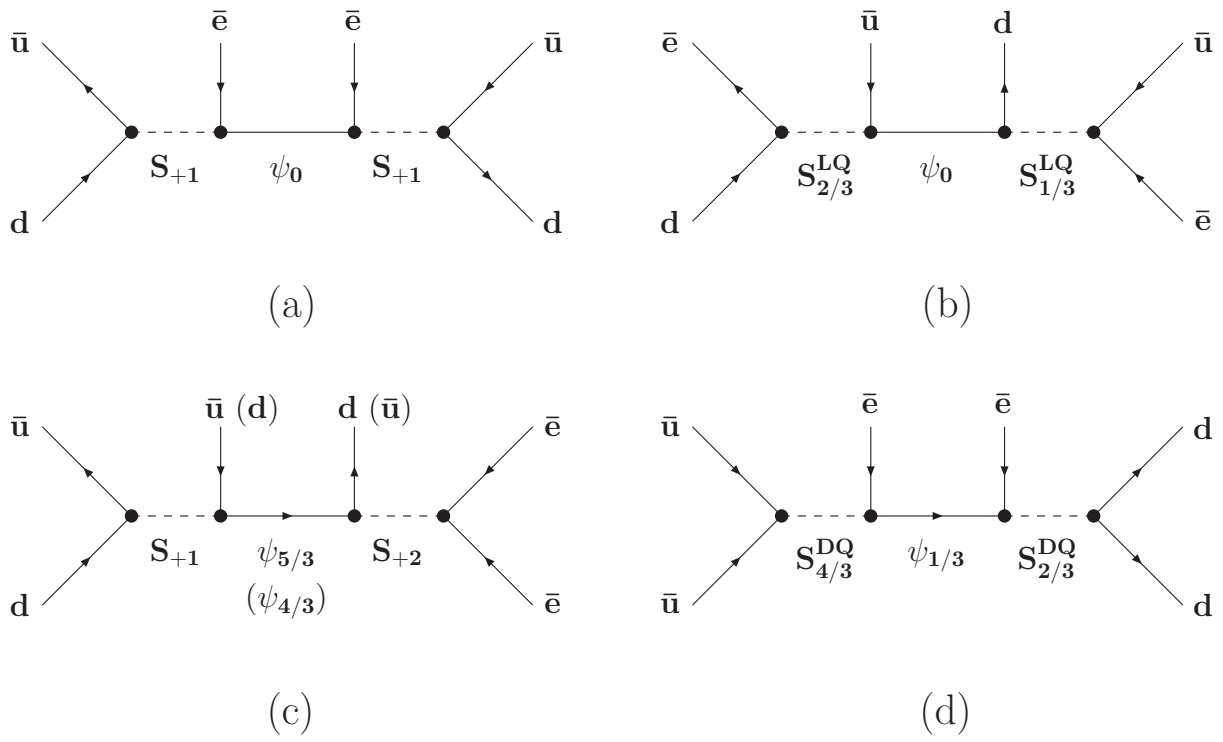

FIG. 3: Example diagrams for short-range double beta decay, see text.

The low-energy energy hadronic and leptonic currents appearing in eq.(2) are defined as:

$$\begin{aligned} J^{\mu}_{V\pm A} &= \overline{u}\gamma^{\mu}(1\pm\gamma_5)d\,, \quad J_{S\pm P} = \overline{u}(1\pm\gamma_5)d\,, \quad J^{\mu\nu} = \overline{u}\sigma^{\mu\nu}d\,, \\ j^{\mu}_{A} &= \overline{e}\gamma^{\mu}\gamma_5 e^c\,, \qquad\qquad j_{S\pm P} = \overline{e}(1\pm\gamma_5)e^c\,. \end{aligned} \tag{3}$$

Note that the vectorial leptonic current $j^{\mu}_{V} = \bar{e}\gamma^{\mu}e^c$ is identically zero. Also the quark tensor operator $\bar{u}\sigma^{\mu\nu}\gamma_5 d$ is not put into the above list since it is reducible to $J^{\mu\nu}$.

The hadronic currents in eq. (3) are expressed in terms of standard operators $(\bar{u}\mathcal{O}d)$, adequate for the description of double beta decay, a low-energy process in which neutrons are converted into protons in a nucleus. The decompositions of table (I), on the other hand, are given in terms of quark currents. The latter can be brought into the standard form, eq. (3) by performing a Fierz transformation, extracting the relevant colour singlet piece(s). The corresponding calculations do depend on the chiralities of the outer fermions.

Once the coefficients for the basic operators of eq.(2) have been calculated for any given decomposition one can write the corresponding inverse half-life as a product of three distinct factors

$$\left(T^{0\nu\beta\beta}_{1/2}\right)^{-1} = G(\sum_i \epsilon_i \mathcal{M}_i)^2. \tag{4}$$

Here, G is the leptonic phase space integral. Numerical values for G can be calculated accurately, see for example [2]. $\mathcal{M}_i$ are the nuclear matrix elements, they are different for the different ϵ_i. Their numerical values for ^{76}Ge can be found in [21], for other isotopes see

[16]. [3]

III. CROSS SECTIONS

In the following we discuss the production cross sections for charged scalars (S_{+1}) and the two different cases each for diquarks ($S^{DQ}_{4/3}$ and $S^{DQ}_{2/3}$) and leptoquarks ($S^{LQ}_{1/3}$ and $S^{LQ}_{2/3}$) as well as their respective antiparticles. These five cross sections, plus the corresponding ones for vectors, are in principle sufficient to test all 18 decompositions of the double beta decay operator in topology-I. The $S^{DQ}_{4/3}$ occurs in decompositions 3-i, 3-ii, 4-ii. The $S^{DQ}_{2/3}$ occurs in 3-i, 3-iii, 5-ii. The leptoquark states $S^{LQ}_{1/3}$ (and $S^{LQ}_{2/3}$) appear in 2-i, 2-iii, and all of 5 (and 2-ii, 2-iii and all of 4, respectively). Finally, S_{+1} appears in all of 1 and in 2-i and 2-ii. Examples of Feynman diagrams are shown in fig. 3 and fig. 4. Note that the list of Feynman diagrams is far from complete.

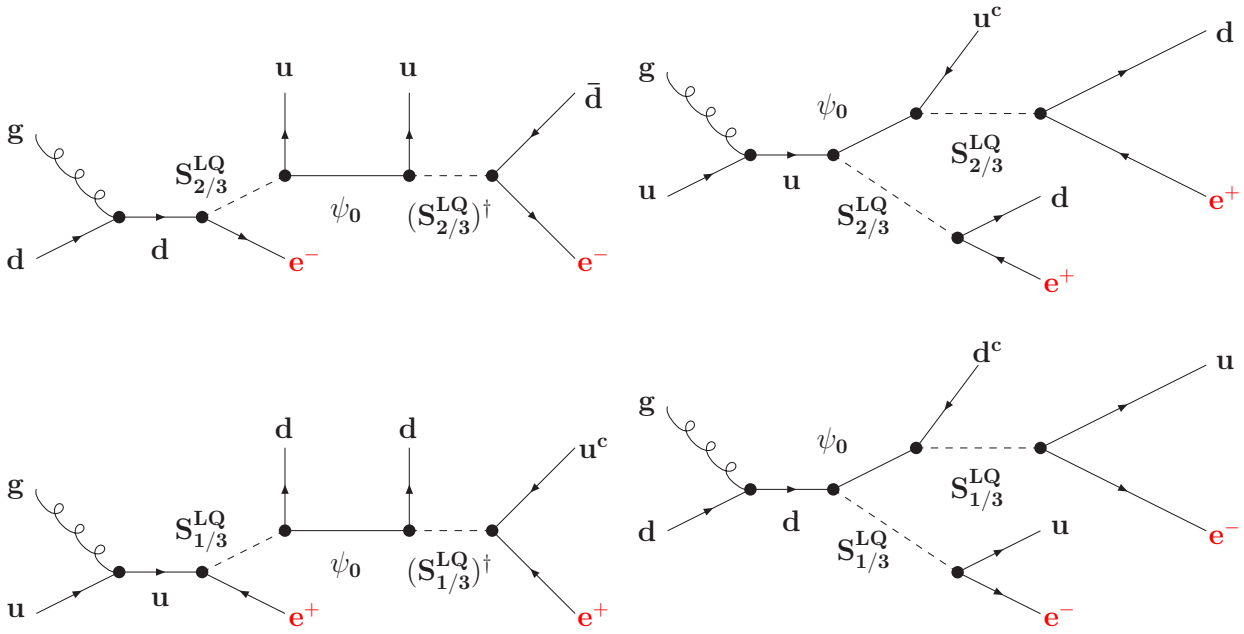

FIG. 4: Example diagrams for single leptoquark production, followed by LNV decay, at the LHC. For discussion see text.

We have implemented the corresponding Lagrangian terms given in Appendix A into CalcHEP [42] and MadGraph5 [43] for the calculation of cross sections. Example results are displayed in figure (5) and (6).

Figure (5) shows cross sections in pb for five different scalars at LHC c.m.s. energy of $\sqrt{s} = 14$ TeV. We show $\sigma(pp \to ee + jets)/(g^2 BR)$, where g stands generically for the coupling entering the production cross section of the scalar, "jets" stands generically for any

[3] For recent review of the nuclear structure theory behind the calculation of $\mathcal{M}_i$ see, for instance, Ref. [41] and references therein.

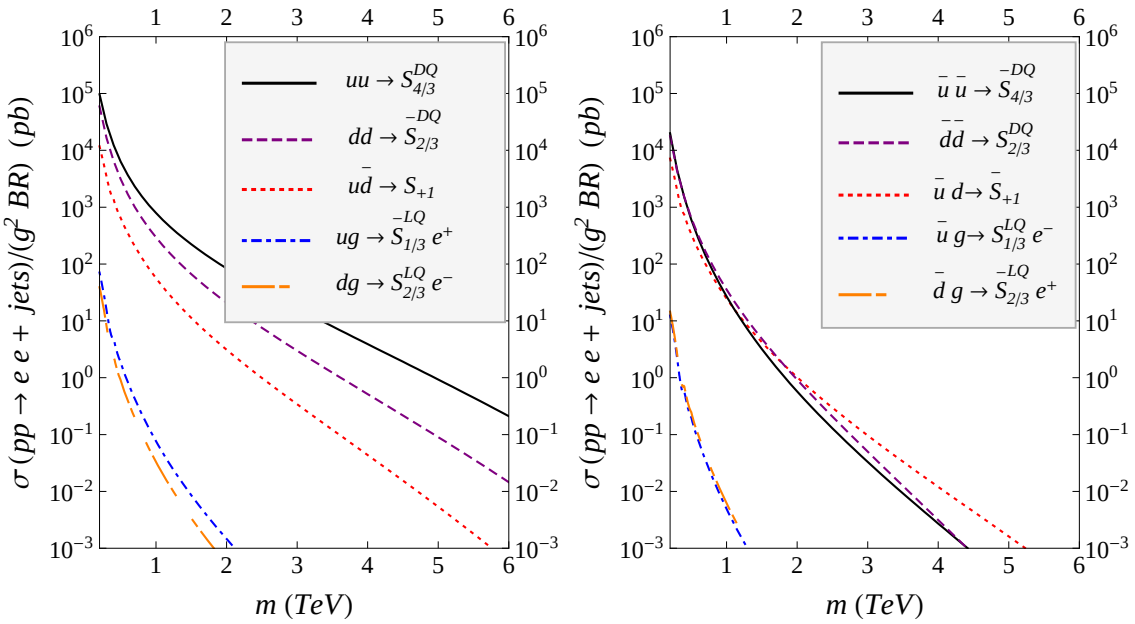

FIG. 5: Production cross sections in pb at the LHC with $\sqrt{s} = 14$ TeV for five different scalars: $S^{DQ}_{4/3}$, $S^{DQ}_{2/3}$, S_{+1}, $S^{LQ}_{1/3}$ and $S^{LQ}_{2/3}$. To the left the production of the scalar being dominantly produced (compare the discussion of the charge asymmetry in V A) is being considered. Depicted at the right is the production cross section for its anti-particle - the scalar with the sub-dominantly produced charge. For S_{+1}, $\sigma(pp \to S_{+1})$ is only a factor $(2 - 3.5)$ larger than $\sigma(pp \to \bar{S}_{+1})$. For other cases much larger ratios are found, for discussion see text.

number of jets, and BR is the branching ratio to the final LNV state. The cross sections shown are for colour sextets in case of diquarks, colour triplets in case of leptoquarks. Note that for scalar diquarks coupling to the same generation of quarks, only the sextet coupling is non-zero. For the charged scalar, S_{+1}, we show the result for the colour singlet. The cross section for a singly charged colour octet is larger by a colour factor of $n_c = 4/3$.

In fig. (5) to the left we show the "dominant-sign" production cross section, while to the right "wrong-sign" charge production cross sections are shown. In case of S_{+1}, $S^{DQ}_{4/3}$ and $S^{LQ}_{1/3}$ the positive sign of the charge has the larger cross section, while for the remaining cases of $S^{DQ}_{2/3}$ and $S^{LQ}_{2/3}$ the negative sign is the dominant production mode. The ratio of dominant to subdominant cross section is, however, different for different scalars: For S_{+1} it is in the range of $(2 - 3.5)$ in the mass range shown, while for the other cases much larger ratios, strongly depending on the mass of the scalar can be found. This "asymmetry" in cross sections forms the basis of the observable "charge asymmetry", which we will discuss later in this paper.

While the charged scalar and the diquark states can be singly produced in an s-channel resonance, as shown in fig. 3, thus leading to large cross sections, in case of leptoquarks the scalar LQ is necessarily always produced in association with a lepton, see fig. 4, explaining the much smaller cross sections seen in fig. 5. While the signal for diquarks (and the charged

scalar) is therefore the "classical" $eejj$-signal with a mass peak in $m^2_{eejj} = m^2_{S_i}$, for LQs the signal is ee with at least three hard jets, a broader distribution in m^2_{eejjj} and a mass peak in $m^2_{e_2jjj} = m^2_{S^{LQ}_j}$, see also section V B.

As shown in fig. (4) leptoquarks can be produced in association with a standard model lepton (electron/positron) or together with one of the exotic fermions, ψ, see table I. We have calculated $\sigma(pp \to S^{LQ}_q + \psi)$ for several different values of m_ψ for both types of LQs (and both types of electric charge). In fig. (6) the results for these cross sections are compared with $\sigma(pp \to S^{LQ}_q + e)$. Usually, $\sigma(pp \to S^{LQ}_q + \psi)$ is smaller than $\sigma(pp \to S^{LQ}_q + e)$, due to the kinematical price of producing a heavy ψ in addition to the heavy LQ. However, for the particular case of $S^{LQ}_{2/3}$, if $m_\psi \ll m_{S^{LQ}_{2/3}}$ the cross section for LQ plus exotic fermion production can be as large (or slightly larger) than $\sigma(pp \to S^{LQ}_q + e)$, because there are twice as many up-quarks in the proton than down-quarks.

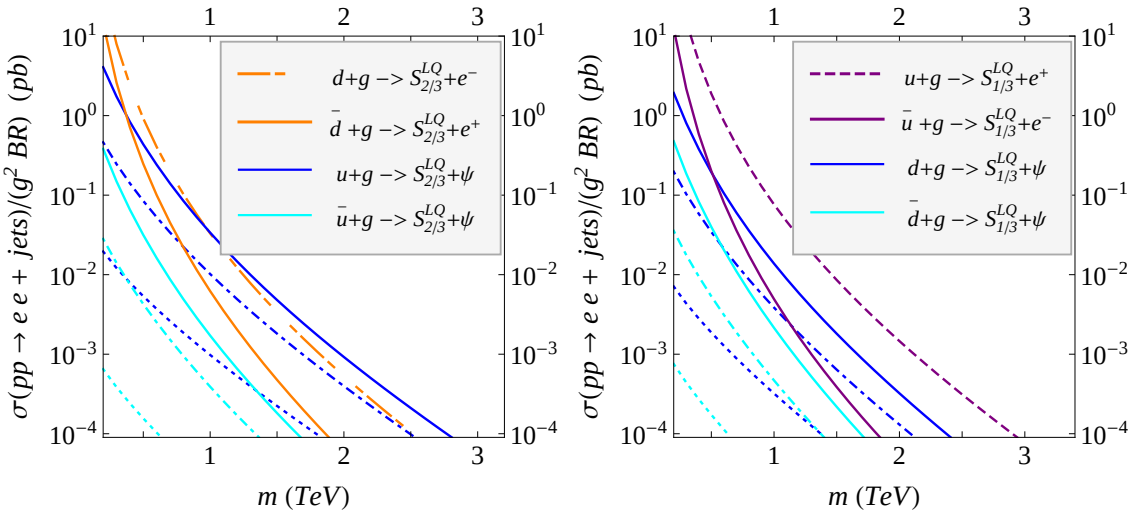

FIG. 6: Production cross sections in pb at the LHC with $\sqrt{s} = 14$ TeV for $S^{LQ}_{2/3}$ (left) and $S^{LQ}_{1/3}$ (right). We show separately cross sections leading to e^-e^- and e^+e^+ final states. For the case of $S^{LQ}_q + \psi$ production, we show cross sections for three different choices of m_ψ: $m_\psi = 0.5$ TeV - full lines; $m_\psi = 1.0$ TeV - dot-dashed lines; $m_\psi = 2.0$ TeV - dotted lines. Usually, $\sigma(pp \to S^{LQ}_q + \psi)$ is smaller than $\sigma(pp \to S^{LQ}_q + e)$, except in the case of $S^{LQ}_{2/3}$ when $m_\psi \ll m_{S^{LQ}_{2/3}}$.

Note, that $\sigma(pp \to S^{LQ}_{2/3} + e^-)$ contributes to e^-e^- type of events, while $\sigma(pp \to S^{LQ}_{2/3} + \psi)$ contributes to e^+e^+ type of events. (Both contribute to e^-e^+ events.) For the $S^{LQ}_{1/3}$ charges of the leptons are reversed, see fig. (4). This will be important for the charge asymmetry, discussed in section V A.

The only boson appearing in the decomposition shown in table I, for which the single production cross section at the LHC is not included in fig. (5), is the doubly charged scalar, S_{+2}. Note, however, that for all decompositions in which S_{+2} appears, the other boson in the diagram is one of the five, for which cross sections are shown in fig. (5). In fact, most

of the decompositions of table I have two different bosons in the left and right part of the diagrams and thus, if both are within reach of the LHC, will lead to multiple "bumps" in the invariant mass distribution of $eejj$ (or e_2jjj), see the discussion in section V B.

Finally, we have also calculated the pair production cross section for $\sigma(pp \to \psi_{1/3}\bar{\psi}_{1/3})$. For coloured fermions at the LHC, the production cross section is dominated by gluon-gluon fusion, thus $\sigma(pp \to \psi_{4/3}\bar{\psi}_{4/3})$ and also $\sigma(pp \to \psi_{5/3}\bar{\psi}_{5/3})$ have very similar values, while for a charge-neutral color octet cross sections are larger than for the case $\sigma(pp \to \psi_{1/3}\bar{\psi}_{1/3})$ by a corresponding colour factor. Pair production of colored fermions provides a different signal as test for double beta decay, since the minimal number of jets here is 4 (compared to 2 or 3 in all other cases). Cross sections are larger than 1 fb up to masses of around 2 TeV and larger than 0.1 fb up to 2.5 TeV. We will also briefly discuss invariant mass peaks for pair production in section V B.

IV. PHENOMENOLOGY

A. Status of related LHC searches

Both, the ATLAS [26] and the CMS [27] collaborations have published searches for events with dilepton plus jets ("$eejj$"). In both cases, limits on right-handed W-bosons and heavy right-handed neutrinos, motivated by the left-right symmetric extension of the standard model [44, 45], have been derived, see fig. (1). The search is based on the assumption that an on-shell W_R is produced, decaying to an on-shell right-handed neutrino, i.e. $W_R \to l_1 N_l \to l_1 l_2 W_R^* \to l_1 l_2 jj$ [28], producing two mass peaks in m_{eejj} and m_{e_2jj}.

The ATLAS collaboration used 2.1 fb^{-1} of statistics at $\sqrt{s} = 7$ TeV and searched for both, like-sign and opposite-sign, dileptons plus any number of jets. A number of cuts are applied to the data, the most important ones for us are: Leptons have to be isolated, with $p_T > 25$ GeV and the dilepton invariant mass m_{ll} is required to be greater than 110 GeV. In addition, at least one jet has to have $p_T > 20$ GeV. For larger mass differences betrween W_R and N, the N is significantly boosted, such that the two jets from the decay $N \to ljj$ are identified as a single jet. Such events are taken into account in the analysis and, according to [26], make up up to half of the signal events. Invariant masses of the m_{lljj} or m_{llj} systems are then required to be larger than 400 GeV.

The main backgrounds have been identified, partially by MonteCarlo (MC) and partially data driven, and depend on the final state (like-sign (SS) versus opposite-sign (OS), as well as electrons versus muons). For like-sign electrons the main background comes from "fake lepton events", i.e. $W + j$, $t\bar{t}$ and QCD multi-jet production, where one or more of the jets is misidentified as an electron. For OS leptons, the main backgrounds are $(Z/\gamma)^* + j$ and $t\bar{t}$ events. The background for OS leptons is larger than for SS leptons by a considerable factor (~ 5), but since rough agreement between MC and actual number of events is found in both cases the resulting upper limits on signal cross sections are similar.

Unfortunately, [26] does not give upper limits on $\sigma \times \mathrm{Br}(eejj)$ as function of m_{eejj}, nor

does ATLAS provide individual data sets for e^-e^- and e^+e^+. Results are instead presented as excluded areas in the plane (m_N, m_{W_R}) for SS+OS (called "Majorana case"), see fig. (1), and OS-only ("Dirac case"), combining muon-type and electron-type events and assuming $g_R = g_L$. [4]

The CMS analysis [27] is based on 3.6 fb^{-1} of data at $\sqrt{s} = 8$ TeV. In their analysis, the leading lepton has to have $p_T > 60$ GeV, the subleading lepton $p_T > 40$ GeV, jet candidates $p_T > 40$ GeV, as well as $m_{ll} > 200$ GeV and $m_{lljj} > 600$ GeV. Events are separated into electron-like and muon-like and separately analysed, but no charge separation within the two sets are given, limits apply to the sum of events in the SS and OS channels. Due to the stronger cuts on the invariant masses, absolute background numbers in the CMS study [27] are similar or smaller than the corresponding background numbers in the ATLAS study [26] despite the larger data sample. Main backgrounds are again $(Z/\gamma)^* + j$ and $t\bar{t}$ events, the number of events from misidentified leptons from QCD is much smaller. The resulting limits in the plane (m_N, m_{W_R}) are stronger than those given by [26], mostly due to the larger statistics (and also larger $\sqrt{s}$).

More important for us is that CMS presents [27] also upper limits on $\sigma \times \mathrm{Br}(eejj)$ as function of m_{eejj}, seperately for electrons and muons. These limits assume $m_N = \frac{1}{2} m_{W_R}$. CMS notes that for this ratio of masses signal acceptance is of order (70-80) % and drops to zero at low m_N, but no information on acceptance as function of m_N is provided. Signal acceptance also becomes small when m_N approaches m_{W_R}, thus for approximately $m_{W_R} - m_N \lesssim 100$ GeV limits disappear. We will use these upper limits in our analysis below. However, we will assume that for the values of fermion masses shown, the acceptance percentage is the same as the one used in the plots shown by CMS. From fig.(2) of [27] one can deduce that this should be a good approximation for fermion masses above $m_F \simeq (200 - 300)$ GeV. Note that [27] shows cross section limits only for $m_{eejj} \geq 1$ TeV. For m_{eejj} larger than about roughly $m_{eejj} \gtrsim 1.7$ TeV limits are of the order (2-3) fb.

In our analysis we will also use estimated sensitivity limits for the future LHC run at $\sqrt{s} = 14$ TeV. We will assume the LHC can collect 300 fb^{-1} of data. Excluding 3 signal events would then optimistically allow to establish an upper limit on $\sigma \times \mathrm{Br}(eejj)$ of $\sigma \times \mathrm{Br}(eejj) \lesssim 0.01$ fb. Such low values are, however, reachable only in regions of parameter space, where background from standard model events is negligible, i.e. at the highest values of m_{eejj}. For lower m_{eejj}, where already in the published data a significant number of background event persists, future data can improve limits only by much weaker factors. We do a simple estimate, which considers that the $t\bar{t}$ production cross section is about a factor

[4] The classification into "Majorana" and "Dirac" case is done, since ATLAS assumes in its analysis that the fermion produced is a heavy neutrino. A Dirac neutrino will remember its lepton number and thus produce only electrons (positrons) in its decay, if the W_R decayed to neutrino plus positron (electron). Thus, for the Dirac case only opposite sign lepton events are produced. An on-shell Majorana neutrino, on the other hand, will decay with 50 % branching ratio into electrons and positrons each, thus producing both SS and OS events.

3 higher at $\sqrt{s} = 14$ TeV than at $\sqrt{s} = 8$ TeV. Thus backgrounds should also be higher by a similar factor. Scaling current limits with this larger background estimate and taking the square root of the statistics (300 fb^{-1} in the future, compared to roughly 3.6 fb^{-1} used in [27], one can estimate the future limit for the region of m_{eejj} in the range of $(1-2)$ TeV very roughly as $\sigma \times \mathrm{Br}(eejj) \lesssim 0.1$ fb.

Finally, as discussed in section III single LQ production at the LHC leads to the final state ee plus at least three hard jets. This case is only partially covered by the searches presented by ATLAS and CMS. In the experimental data sets the number of jets is required to be larger or equal to one, including in principle events with 1, 2 and more jets. This is done simply because for large mass hierarchies $m_{S_i} \gg m_\psi$, the fermion is boosted and thus two jets coming from the decay of ψ might be visible as a single jet only. On the other hand, while events with more than two hard jets are included in this data set, the system ee plus any number of jets does not form a mass peak in case of LQs, as already mentioned. Peaks in $m^2_{e_2jjj}$, as expected for the LQs have not been searched for in [26, 27]. However, one can assume that such a search ($ee + 3j$ with peak in $m^2_{e_2jjj}$) should actually have similar or smaller backgrounds, due to the larger number of jets, than the search presented in [26, 27]. In our analysis we will therefore assume also in this case that in the future limits of order $(0.1-1)$ fb will be reached. More precise numbers would require a full MonteCarlo simulation of signals and backgrounds, which is beyond the scope of the present work. Instead, see below in section IV C, we estimate how our limits will change as a function of the number of excluded events.

B. Status and future of $0\nu\beta\beta$ limits

As mentioned in the introduction, currently the best limits on $0\nu\beta\beta$ decay come from experiments on two isotopes, namely ^{76}Ge and ^{136}Xe. The Heidelberg-Moscow collaboration gives $T^{0\nu\beta\beta}_{1/2}(^{76}\mathrm{Ge}) \geq 1.9 \cdot 10^{25}$ yr [23], while the recent results from EXO-200 and KamLAND-ZEN quote $T^{0\nu\beta\beta}_{1/2}(^{136}\mathrm{Xe}) \geq 1.6 \cdot 10^{25}$ yr [24] and $T^{0\nu\beta\beta}_{1/2}(^{136}\mathrm{Xe}) \geq 1.9 \cdot 10^{25}$ yr [25], both at the 90 % CL. However, it is expected that these limits will be improved within the near future. The GERDA experiment [46, 47] will release first $0\nu\beta\beta$ data in summer of 2013 and then move to "phase-II", aiming for $T^{0\nu\beta\beta}_{1/2}(^{76}\mathrm{Ge})$ in excess of 10^{26} yr. An experiment using ^{130}Te in bolometers named CUORE [48], with senstivity order 10^{26} yr is currently under construction. Proposals for ton-scale next-to-next generation $0\nu\beta\beta$ experiments claim that even sensitivities in excess $T^{0\nu\beta\beta}_{1/2} \sim 10^{27}$ yr can be reached for ^{136}Xe [49, 50] and ^{76}Ge [46, 51]. For recent reviews and a list of experimental references, see for example [52].

In table (II) we therefore quote current and expexcted future limits on M_{eff} from double beta decay experiments using $T^{0\nu\beta\beta}_{1/2}(^{136}\mathrm{Xe}) \geq 1.6 \cdot 10^{25}$ yr (current) and 10^{27} yr (future). Here, M_{eff} and g_{eff} are simply defined as the effective mass and couplings, which enter the

Decomposition #	$S - S'$	current limit:	future limit:
1-i, 1-ii	$S^{(1)}_{+1} - S^{(1)}_{+1}/S_{+2}$	1.4	2.1
1-i, 1-ii	$S^{(8)}_{+1} - S^{(8)}_{+1}/S_{+2}$	2.5-3.1	3.7-4.6
2-i, 2-ii	$S^{(1)}_{+1} - S^{LQ}_{i}$	1.2-1.4	1.8-2.2
2-i, 2-ii	$S^{(8)}_{+1} - S^{LQ}_{i}$	2.2-2.7	3.2-4.0
2-iii	$S^{LQ}_{i} - S^{LQ}_{j}$	1.6-3.1	2.4-4.6
3-i, 3-ii, 3-iii	$S^{DQ}_{i} - S^{DQ}_{j}/S_{+2}$	2.4-2.7	3.5-4.1
4-i, 5-i	$S^{LQ}_{i} - S^{LQ}_{i}$	2.0-2.5	3.0-3.7
4-ii, 5-ii	$S^{DQ}_{i} - S^{LQ}_{j}$	2.0-2.4	3.0-3.5

TABLE II: *Status and future of limits on short-range operators from $0\nu\beta\beta$ decay experiments. Different decompositions result in different limits and depend on the helicity of the outer fermions. The first column gives the decompositon number, compare to table (I), the 2nd column indicates the exchanged scalars. If within a certain (set of) decomposition(s) more than one operator can appear, depending on helicity asignments, for brevity we quote a range for the limit corresponding to the largest and smallest operators within this decomposition. "Current limit" are the limits assuming $T^{0\nu\beta\beta}_{1/2}(^{136}Xe) \geq 1.6 \times 10^{25}$ yr [24], while "future limit" correspond to an assumed future limit of the order of 10^{27} yr. The numbers quoted are limits on M_{eff} in TeV and scale as $g^{(4/5)}_{eff}$.*

$0\nu\beta\beta$ decay amplitude:

$$M_{eff} = (m_S^2 m_\psi m_{S'}^2)^{(1/5)} \qquad (5)$$
$$g_{eff} = (g_1 g_2 g_3 g_4)^{(1/4)}$$

We show limits for the different decompositions assuming scalars are exchanged. The limits on M_{eff} are in TeV and scale as $g^{(4/5)}_{eff}$. Within a given decomposition different operators can appear in the calculation of the $0\nu\beta\beta$ decay half-live. If within a given decomposition there is more than one operator combination that appears for the different possible helicity states, we quote a range of limits, corresponding to the operators with the largest and smallest possible rate within this decomposition. Numbers are calculated using the nuclear matrix elements of [16] and the uncertainty on M_{eff} scales as $\Delta(M_{eff}) \propto (\Delta M_{\rm Nucl.})^{(1/5)}$, where $M_{\rm Nucl}$ stands generically for the nuclear matrix elements. Current limits range from $M_{eff} \gtrsim 1.2 - 3.1$ TeV, future sensitivities up to $M_{eff} \gtrsim 1.8 - 4.6$ TeV are expected.

C. LHC vs $0\nu\beta\beta$: Numerical analysis

In this section we compare the LHC and $0\nu\beta\beta$ sensitivities of the different decompositions for $0\nu\beta\beta$. In the numerical analysis we will develop in this section we will concentrate on the case when the fermion mass is smaller than (one of) the scalar masses. The numerical

analysis of the case when the fermion mass is larger than the scalar masses will be analysed in a future paper.

We can divide the discussion of all 18-decompositions into two group of cases. The first group correspond to "symmetric " and "like-symmetric" decompositions. The former are simply those decompositions, in which a scalar with the same quantum numbers appears twice in the diagram (1-i, 5-i, 4-i), while the later are those with two different scalars but of the same kind (two different leptoquarks or two different diquarks: 2-iii, 3-i). The second group correspond to "asymmetric" decompositions. Those correspond to decompositions with S_{+2} and either a S_{+1} or a diquark (1-ii, 3-ii, 3-iii) and decompositions with a leptoquark and either a S_{+1} or a diquark (2-i, 2-ii, 4-ii, 5-ii).

First we will derive limits from existing LHC data at $\sqrt{s} = 8$ TeV to compare then the discovery potential of the forthcoming $\sqrt{s} = 14$ TeV phase of the LHC with the sensitivity of current and future $0\nu\beta\beta$ decay experiments. We will begin our discussion with the "symmetric" decomposition $(\bar{u}d)(\bar{e})(\bar{e})(\bar{u}d)$.

As discussed in section IV-A the most stringent current limits from the LHC on like-sign lepton searches come from data taken by the CMS collaboration at $\sqrt{s} = 8$ TeV [27]. CMS presents also upper limits on $\sigma \times Br(eejj)$ as a function of m_{eejj}. These limits apply directly to the case of the decomposition $(\bar{u}d)(\bar{e})(\bar{e})(\bar{u}d)$, which describes at LHC a produced scalar S_{+1}, decaying to $S_{+1} \to \psi_0 e^+$, followed by $\psi_0 \to e^+\bar{u}d$, producing two mass peaks in m_{eejj} and m_{e_2jj}.

The number of eejj-like events at the LHC in general depends on a different combination of couplings and masses than the $0\nu\beta\beta$ decay amplitude. The $0\nu\beta\beta$ half-life depends on the effective parameters defined in Eq. (5) and the cross section $\sigma \times Br(eejj)$ is, in the narrow width approximation, proportional to $g^2_{udS_{+1}}$ and to a non trivial function $F_{S_{+1}}$ of the scalar mass $m_{S_{+1}}$ We can then write the number of events as:

$$\sigma \times Br(eejj) = \sigma(pp \to S) \times \mathrm{Br}(S \to eejj) = F_S\,(m_S)\, g_1^2\ \mathrm{Br}(S \to eejj), \tag{6}$$

defining

$$F_{S_{+1}}(m_{S_{+1}}) = \sigma(pp \to S_{+1})/g^2_{udS_{+1}}. \tag{7}$$

The $\mathrm{Br}(S \to eejj)$ can be calculated from eq. (A.2) and is equal to

$$Br(S \to eejj) = \frac{f(m_\psi/m_S)g_2^2}{3g_1^2 + f(m_\psi/m_S)g_2^2} \times \frac{1}{2}. \tag{8}$$

Here $S = S_{+1}$, $g_1 = g_{udS_{+1}}$, $g_2 = g_{e\psi_0 S_{+1}}$, $\psi = \psi_0$ and $f(x) = (1-x^2)^2$. Note that in the limit where all couplings are equal (and $m_{\psi_0} = 0$) $\mathrm{Br}(S_{+1} \to e^+e^+jj) = \mathrm{Br}(S_{+1} \to e^+e^-jj) \simeq 1/8$. We have used CalcHEP [42] to calculate the production cross sections for S_{+1} at the LHC. We have plotted our results in Fig. 5 and compared them with the literature [29] finding quite good agreement.

In "symmetric" decompositions, such as $(\bar{u}d)(\bar{e})(\bar{e})(\bar{u}d)$, the effective couplings and scalar boson masses are pairwise equal, i.e. in Eq. (5) $g_1 = g_4$, $g_2 = g_3$ and $m_S = m_{S'}$. Then, the

effective parameters defined in (5) become:

$$M_{eff(S)} \;=\; (m_S^4 m_\psi)^{1/5}, \;\; g_{eff(S)} = (g_1 g_2)^{1/2}. \tag{9}$$

Eq. (6) depends on 4 variables: the couplings g_1, g_2 and the masses m_S, m_ψ. For comparison with $0\nu\beta\beta$ we have expressed Eq. (6), using Eq. (9) and (8), in terms of 4 new variables: the effective coupling and mass g_{eff}, M_{eff}, the fermion mass m_ψ and the $Br(S \to eejj)$. Then, using Eq. (6) expressed in terms of this 4 new variables, and the current limits on $\sigma \times Br(eejj)$ presented by CMS [27] we can plot in the plane g_{eff} versus M_{eff} bounds of the LHC for differentt values of the $Br(S_{+1} \to eejj)$ and the fermion mass m_{ψ_0}. We have drawn these limits for $Br(S_{+1} \to eejj) = 10^{-1}$ (solid red lines) and $Br(S_{+1} \to eejj) = 10^{-2}$ (dashed red lines) in Fig. 7 using different values of the fermion mass $m_{\psi_0} = 200$ GeV, 800 GeV. For larger masses m_{ψ_0} the LHC limits become more stringent except for the region $(m_{\psi_0} - m_{S_{+1}}) \lesssim 100$ GeV, where the LHC sensitivity becomes very small as we discussed in section IV A. Note, that the for the dotted/dashed lines, the part of the line, which is shown dotted correspond to values of $1 \leq g_1 = g_{udS_{+1}} \leq 2$, i.e. close to values where this coupling would become non-perturbative.

In addition, Fig. 7 shows current and future limits from $0\nu\beta\beta$ decay. The dark gray area is the currently excluded part of parameter space from non-observation of ^{136}Xe decay with $T_{1/2}^{0\nu\beta\beta} \geq 1.6 \times 10^{25}$ ys [24] and the blue area correspond to an assumed future $0\nu\beta\beta$ decay sensitivities of $T_{1/2}^{0\nu\beta\beta} \geq 10^{27}$ ys. We have used as a current limit $M_{eff} > 1.2\ TeV \times g_{eff}^{4/5}$ and for future sensitivities up to $M_{eff} > 4.6\ TeV \times g_{eff}^{4/5}$. These correspond to the most pessimistic case for the current sensitivity of $0\nu\beta\beta$ decay and the most optimistic reach for $0\nu\beta\beta$ decay in the foreseeable future (See Table II). As we can see from Fig. 7 the LHC is already competitive to $0\nu\beta\beta$ for part of the parameter region of the decomposition $(\bar{u}d)(\bar{e})(\bar{e})(\bar{u}d)$, especially for larger masses of m_{ψ_0}. However, this mechanism is not ruled out, quite on the contrary, most of the parameter region explored by future $0\nu\beta\beta$ decay experiments has not been covered yet.

Now we will analyze the discovery potential of the forthcoming $\sqrt{s} = 14$ TeV phase of the LHC. We will start our discussion with the first group of decompositions, i.e. "symmetric" and "like-symmetric" decompositions. Recall, for "symmetric" decompositions one can use Eqs. (6)-(9) to describe the cross section $\sigma \times Br(eejj)$ in terms of the effective masses and couplings relevant for $0\nu\beta\beta$. In the LQ case, the LQ is produced in association with a lepton, i.e. in Eq. (6) we calculate $\sigma(pp \to S^{LQ} + e) \times \mathrm{Br}(S^{LQ} \to ejjj)$. For "like-symmetric" decompositions, Eq. (9) is also a good approximation. This is because both LQs or both diquarks can be produced at LHC and in turn will have similar limits on the masses $m_S, m_{S'}$ and couplings g_1, g_4 and g_2, g_3. We have used CalcHEP [42] and MadGraph 5 [43] to calculate the production cross sections for S_{+1}, S^{LQ}, and S^{DQ} at the LHC. We have plotted our results in Fig. 5 and compared them with the literature [29, 40, 53] and found quite good agreement in all cases.

In Fig. 8, 9 we then plot the sensitivities of $0\nu\beta\beta$ decay and the LHC for five different cases in the plane g_{eff} versus M_{eff}. For the LHC we show the expected sensitivity limits, assuming

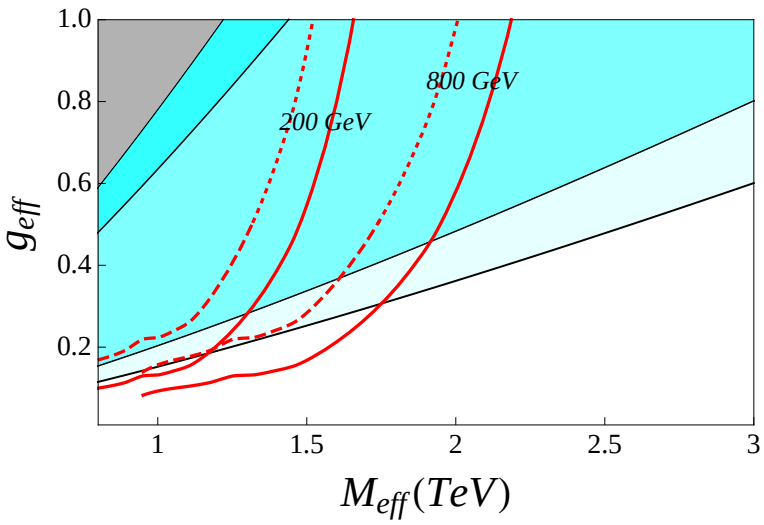

FIG. 7: Current limits for the LHC at $\sqrt{s} = 8$ TeV for production of scalars S_{+1} compared with current and future double beta decay experiments. The gray region in the top left corner is ruled out by current $0\nu\beta\beta$ data. The blue region represents the parameter region accessible in near future $0\nu\beta\beta$ experiments, whereas the red lines shows current LHC limits for production of scalars S_{+1}. Solid red lines were calculated using $Br(S_{+1} \to eejj) = 10^{-1}$ while the dashed and dotted red lines were calculated using $Br(S_{+1} \to eejj) = 10^{-2}$ for different values of the fermion mass $m_{\psi_0} = 200$ GeV, 800 GeV, see text.

less then 3 signal events in 300 fb^{-1} of statistics, and plot for two values of Br($S \to eejj$), i.e 10^{-2} (dashed lines) and 10^{-1} (solid lines) , for two different values of $m_\psi = 200$ GeV (left) and $m_\psi = 1$ TeV (right). Again, for larger masses m_ψ the LHC limits become more stringent except for the region $(m_\psi - m_S) \lesssim 100$ GeV, where the LHC sensitivity is low. The different color codes correspond to the five different scalar bosons, that can be singly produced at the LHC, namely S_{+1} (red), $S^{DQ}_{4/3}$ (black), $S^{DQ}_{2/3}$ (purple), $S^{LQ}_{2/3}$ (blue) and $S^{LQ}_{1/3}$ (orange). In Fig. 8 we have ploted three cases which correspond to the scalars S_{+1}, $S^{DQ}_{4/3}$ and $S^{DQ}_{2/3}$ while in Fig. 9 we have plotted the remaining two leptoquark cases $S^{LQ}_{2/3}$ and $S^{LQ}_{1/3}$. In addition Figs. 8, 9 show four different cases for current and future limits from $0\nu\beta\beta$ decay. The dark gray area is, as in fig 7, the currently excluded part of parameter space from non-observation of ^{136}Xe decay with $T^{0\nu\beta\beta}_{1/2} \geq 1.6 \times 10^{25}$ ys [24] assuming $0\nu\beta\beta$ decay is caused by the decomposition with the smallest rate (see Table II), and thus corresponds to the most pessimistic case for the sensitivity of $0\nu\beta\beta$ decay. The three blue areas are (from left to right): Smallest rate, but for a limit of $T^{0\nu\beta\beta}_{1/2} \geq 10^{26}$ ys, largest rate with $T^{0\nu\beta\beta}_{1/2} \geq 10^{26}$ ys and, finally the largest rate with $T^{0\nu\beta\beta}_{1/2} \geq 10^{27}$ ys. The lightest area to the right therefore corresponds to the most optimistic reach for $0\nu\beta\beta$ decay in the foreseeable future.

As can be seen from Figs. 8, 9, with the exception of the LQ cases (Fig. 9), the LHC at $\sqrt{s} = 14$ TeV will be more sensitive than $0\nu\beta\beta$ decay experiments as probe for LNV. For the LQ case, the LHC is more sensitive than $0\nu\beta\beta$ decay in the pessimistic case for $0\nu\beta\beta$

(operators $\mathcal{O}_1$ and $\mathcal{O}_5$ in the notation of [21]) but not for the one to which $0\nu\beta\beta$ decay is most sensitive, particularly $\mathcal{O}_2$. For the remaining operators $\mathcal{O}_3$ and $\mathcal{O}_4$ $0\nu\beta\beta$ decay and LHC sensitivities are very similar.

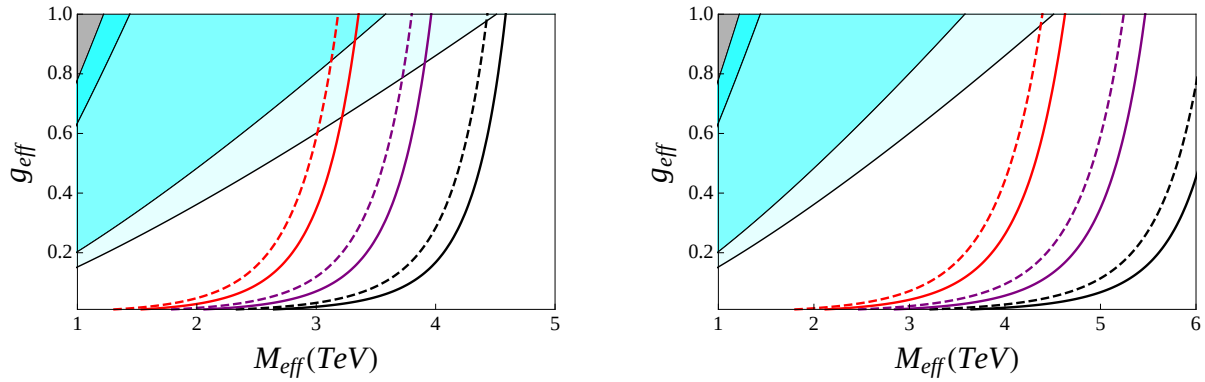

FIG. 8: Future limits for the LHC at $\sqrt{s} = 14$ TeV compared with current and future double beta decay experiment. The gray region on the top left corner is ruled out by $0\nu\beta\beta$. The blue region represents the parametric region accessible in near future $0\nu\beta\beta$ experiments, whereas the colored lines shows sensitivity limits for the LHC for production of three different scalar bosons S_{+1} (red), $S^{DQ}_{2/3}$ (purple) and $S^{DQ}_{4/3}$ (black). Solid lines were calculated using $Br(S \to eejj) = 10^{-1}$ whiles dashed lines were calculated using $Br(S \to eejj) = 10^{-2}$ for different values of the fermion mass $m_\psi = 200$ GeV (left) and $m_\psi = 1000$ GeV (right).

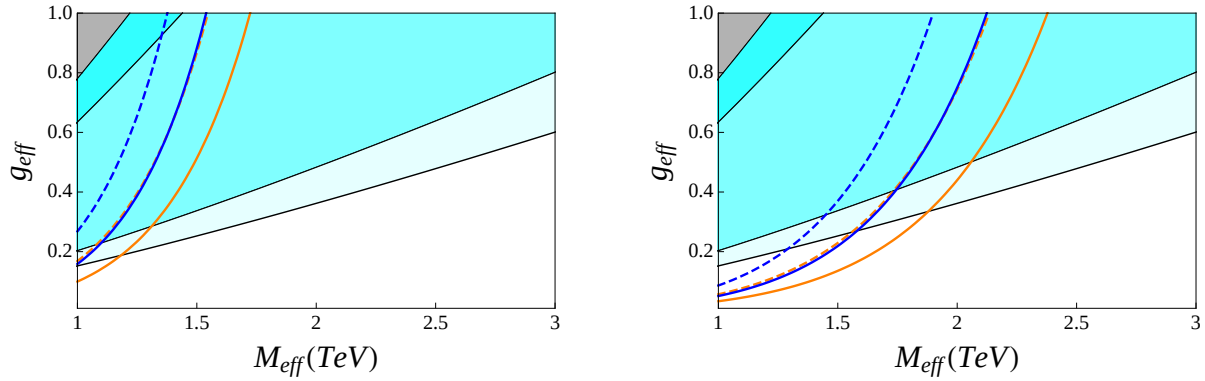

FIG. 9: As fig. 8, but for production of two leptoquark scalars $S^{LQ}_{2/3}$ (blue) and $S^{LQ}_{1/3}$ (orange). Note, that the dashed line for $Br(S \to eejj) = 10^{-2}$ in case of $S^{LQ}_{1/3}$ is very similar to $Br(S \to eejj) = 10^{-1}$ for the case of $S^{LQ}_{2/3}$.

Now we will discuss the second group of decompositions, which correspond to the "asymmetric" cases, with two different scalar masses and all couplings different. In this case, the assumption $g_1 = g_4$, $g_2 = g_3$ and $m_S = m_{S'}$ in Eq. (9) is violated and the plane g_1^2 vs m_S is more adequate for comparison of LHC and $0\nu\beta\beta$ decay sensitivities.

In Fig. 10 we then compare the sensitivities of $0\nu\beta\beta$ decay and the LHC for three different cases, using Eq. (6). The different color codes correspond to the three different scalar bosons, that can be singly produced at the LHC, namely S_{+1} (red), $S^{DQ}_{4/3}$ (black), $S^{DQ}_{2/3}$ (purple). For the LHC we show the expected sensitivity limits for $Br(S \to eejj) = 10^{-1}$ (solid lines) in the plane g_1 versus m_S.

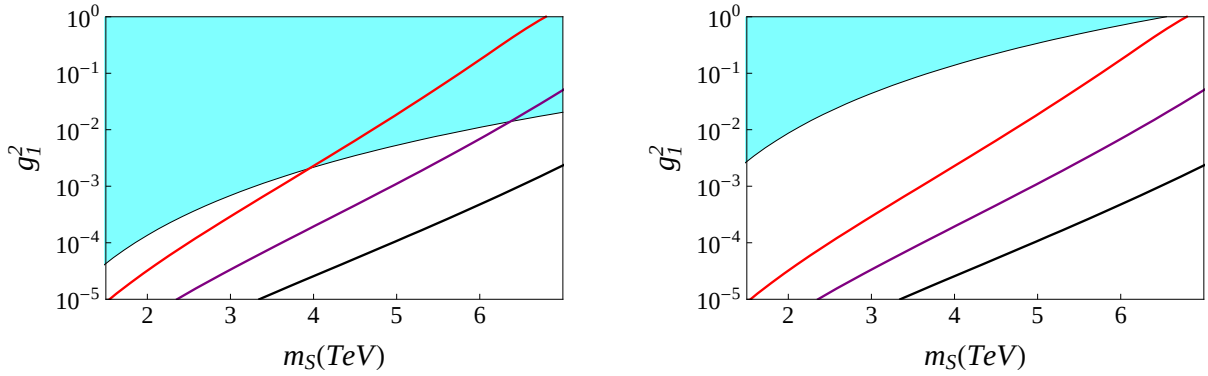

FIG. 10: Future limits for the LHC at $\sqrt{s} = 14$ TeV compared with future double beta decay experiments. The blue region represents the parameter region accessible in near future $0\nu\beta\beta$ experiments, whereas the colored lines shows sensitivity limits for the LHC for production of three different scalar bosons S_{+1} (red), $S^{DQ}_{2/3}$ (purple) and $S^{DQ}_{4/3}$ (black). Solid lines were calculated using $Br(S \to eejj) = 10^{-1}$ and the blue region was calculated using $m_\psi = 1.5$ TeV, $m_{S'} = 2.0$ TeV, $g_2 = g_3 = g_4 = 1$ (left) and $g_2 = g_3 = g_4 = 0.5$ (right).

Fig. 10 shows future limits from $0\nu\beta\beta$ decay which corresponds to the most optimistic reach for $0\nu\beta\beta$ decay in the foreseeable future. Those limits were calculated using, in Eq. (5), $m_\psi = 1.5$ TeV , $m_{S'} = 2.0$ TeV, $g_2 = g_3 = g_4 = 1$ (left) and $g_2 = g_3 = g_4 = 0.5$ (right). For larger masses $m_\psi, m_{S'}$ or smaller couplings g_2, g_3, g_4 those limits become weaker. The choice of $m_\psi = 1.5$ TeV, $m_{S'} = 2.0$ TeV is reasonable since all the "asymmetric" decompositions must have coloured fermions and these can be constrained through pair production searches, which will yield sensitivity limits on their masses of $2 - 2.5$ TeV. Moreover in the "asymmetric" decompositions the scalar S' is a leptoquark or a S_{+2}. Also for leptoquarks the LHC searches from pair and single productions [54] will have sensitivities around 2 TeV and the doubly charged scalar S_{+2} can also be searched trough pair production (through a production graph with a virtual photon). As can be seen from Fig. 10 the LHC at $\sqrt{s} = 14$ TeV will be more sensitive than $0\nu\beta\beta$ decay experiments as probe for LNV for all the "asymmetric" decompositions.

Finally we have compared in Fig. 11 sensitivity limits for the "symmetric" decomposition $(\bar{u}d)(\bar{e})(\bar{e})(\bar{u}d)$ assuming 3, 10 and 30 events in $300 fb^{-1}$ of statistics. As one can see from Fig. 11 even under the pessimistic assumption that only 30 signal events can be excluded, our previous limits calculated for the more optimistic situation of 3 events (see Fig. 8) suffer only minor changes (in this linear plot) and the LHC is still more sensitive than $0\nu\beta\beta$. More accurate numbers of the total number of events necessary to claim discovery/exclusion

would require a full detector MonteCarlo, outside the scope of this paper.

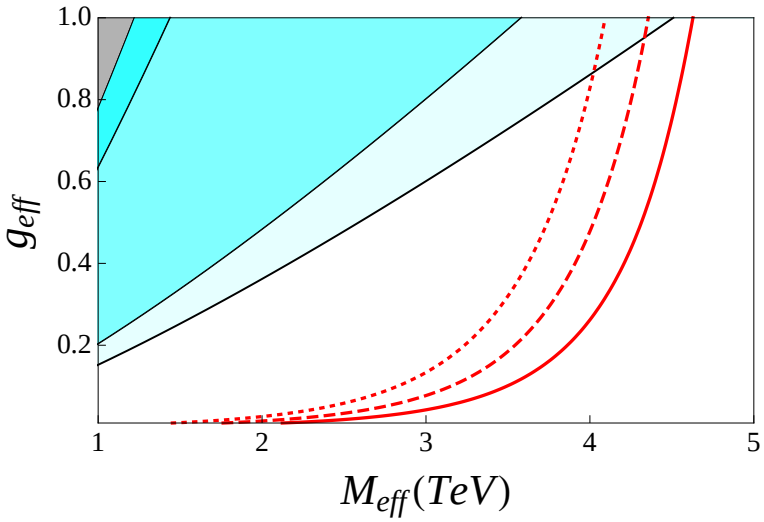

FIG. 11: Comparison of expected sensitivity limits assuming less than 3 (solid), 10 (dashed) and 30 (dotted) signal events in $300 fb^{-1}$ of statistic at LHC for the production of the scalar bosons S_{+1}. Red lines were calculated using $Br(S \to eejj) = 10^{-1}$ and fermion mass $m_{\psi_0} = 1000$ GeV. The gray region on the top left corner is ruled out by $0\nu\beta\beta$ whereas the blue region represents the parametric region accessible in near future $0\nu\beta\beta$ experiments. See text for more details.

V. DISTINGUISHING LNV MODELS AT THE LHC

In the previous section we have compared the sensitivity of the LHC with $0\nu\beta\beta$ decay. Here, we discuss the question how the different LNV decompositions could actually be distinguished using LHC data, if a positive signal were to be found in the $\sqrt{s} = 14$ TeV run. We will consider two types of observables: (i) charge asymmetry [5] and (ii) invariant mass peaks. Interestingly, the combination of the two sets of observables is sufficient to distinguish among nearly all decompositions. The only exceptions are the pairs of cases (1-ii-a)-(1-ii-b) and (1-i)-(3-i), the latter, however, only in the "mass-degenerate" limit, see below.

Recall first that the scalars S_{+1}, $S^{DQ}_{4/3}$ and $S^{DQ}_{2/3}$ are produced in s-channel, while single leptoquarks are produced at the LHC always in association with a lepton. The LQ final state that we are interested in, is therefore $eejjj$, different from the other cases, see discussion next section. We will therefore separate the discussion here in "LQ-like" and other cases.

[5] This charge asymmetry has also been discussed in a different context in the recent paper [55].

A. Charge asymmetry

In the dilepton event samples, there are three subsets of events with different charges: e^+e^+, e^+e^- and e^-e^-. From these three numbers we can form two independent ratios:

$$x_{CA} = \#(e^+e^+)/\#(e^-e^-) \qquad (10)$$
$$y_{CA} = \#(e^-e^+)/\#(e^+e^+).$$

Consider the simpler case of y_{CA} first. In the cases where the fermion in the diagram is neutral, $\psi = \psi_0$, it is a Majorana particle and at tree-level $\mathrm{Br}(\psi_0 \to e^+jj) = \mathrm{Br}(\psi_0 \to e^-jj)$. [6] Thus, all decompositions with ψ_0 will have $y_{CA} = 1/2$, up to loop corrections. The situation is different for decompositions with charged fermions. Here we can distinguish the cases involving $\psi_{4/3}$ and $\psi_{5/3}$, on the one hand, and $\psi_{1/3}$ on the other hand. Since $\psi_{4/3}$ and $\psi_{5/3}$ can decay only into e^+e^+j and e^-e^-j, all decompositions involving these fermions have $y_{CA} = 0$. Finally, $\psi_{1/3}$ can decay into both charge signs, but the branching ratio of $\psi_{+1/3}$ into positrons and electrons involve different combinations of couplings (and masses), and therefore are free numbers. y_{CA} in this case is arbitrary, but could be used to fix some combination of couplings experimentally.

We now turn to the discussion of x_{CA}. Define the ratio for the LHC production cross section of one of our five scalars, relative to the cross section for its charge conjugate state as:

$$R_\sigma^{S_i} = \frac{\sigma(pp \to S_i)}{\sigma(pp \to \bar{S}_i)}, \qquad (11)$$

Here, S_i stands for any of $S_i = S_{+1}, S^{DQ}_{4/3}, S^{DQ}_{2/3}, S^{LQ}_{2/3}, S^{LQ}_{1/3}$. We can divide the discussion of all 18 decompositions into three groups of cases. We put into the first group the six decompositions without any leptoquark in the diagram, i.e. all decompositions T-I-i and T-I-iii of table I. Into the second group we put the decompositions with two leptoquarks, i.e. 2-iii, 4-i and 5-i. The remaining 8 decompositions with one leptoquark form the third group.

We start the discussion with group-(1). As shown in fig. (5), $R_\sigma^{S_i}$ is different for the various scalars and moreover strongly dependent on the mass of the scalar. [7] This asymmetry in cross sections will cause the charge asymmetry x_{CA} to depend strongly on the decomposition. The charge asymmetry x_{CA} is shown in fig. 12 for diquarks and for S_{+1}. Consider first the case denoted S_{+1} on the left. This corresponds to both, the case 1-i and the two sub-cases 1-ii-a and 1-ii-b. The former is an example of a symmetric decomposition, i.e. here two of the four couplings in the diagram are pairwise equal, namely $g_{S_{+1}\bar{u}d}$ connecting two outer legs and and $g_{S_{+1}\bar{e}\psi_0}$ connecting two propagators in either beta decay subprocess to the left and to the right. It is straightforward to show that upon calculating x_{CA} all couplings cancel out an x_{CA} simply is $x_{CA}^{\mathrm{sym}} = R_\sigma$. Thus, for symmetric decompositions, x_{CA} at any fixed

[6] The branching ratios equal 1/2 in case there is no generation mixing.
[7] Note that $R_\sigma^{V_i}$ for vectors will behave exactly as $R_\sigma^{S_i}$ discussed here.

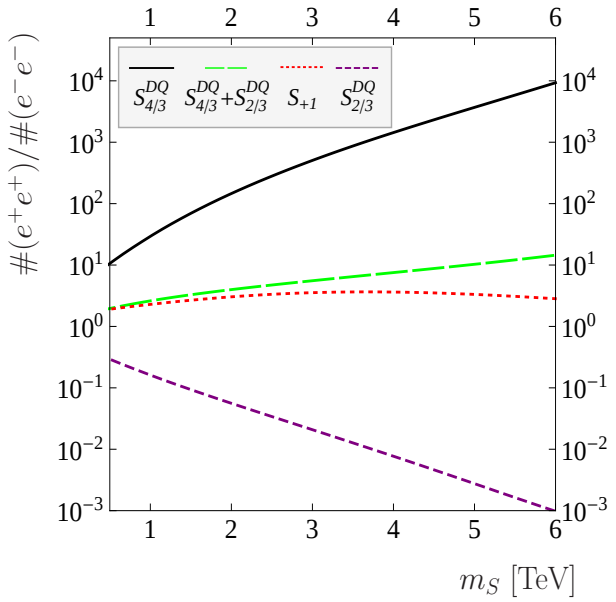

FIG. 12: Charge asymmetry x_{CA}, see eq. (10), as a function of the boson mass for different kinds of scalars. Shown are the cases with S_{+1} or diquarks, for discussion see text.

mass of the scalar is simply a number, predicted by the decomposition. [8] The two sub-cases 1-ii-a and 1-ii-b can be called "absolutely asymmetric" decompositions, since the S_{+2} can not be singly produced in the LHC. In these cases only the couplings at the S_{+1} vertices matter and drop out again in the calculation of x_{CA}. Thus, the line denoted S_{+1} in fig. (12) is valid for both, decomposition 1-i and 1-ii.

Consider DQs, i.e. decompositions 3-i, 3-ii and 3-iii. The lines denoted $S^{DQ}_{4/3}$ and $S^{DQ}_{2/3}$ in fig. (12) correspond to decompositions 3-ii and 3-iii. In these two cases the decomposition is "completely asymmetric" and therefore does not depend on the values of individual couplings, but depends strongly on the mass of the scalar.

For decomposition 3-i the discussion is slightly more complicated. Here, one can distinguish the case where the two diquark masses are degenerate ($m_{S^{DQ}_{4/3}} = m_{S^{DQ}_{2/3}}$) and the non-degenerate case. In the non-degenerate case the distributions in m^2_{eejj} would show two distinct peaks, one having the x_{CA} appropriate for $S^{DQ}_{4/3}$ while the other has x_{CA} of $S^{DQ}_{2/3}$. In fact, such a non-degenerate case is not only "easy" to resolve from the decomposition(s) involving S_{+1}, having more than one peak in m^2_{eejj} would actually allow to probe for all four couplings entering the diagram and thus provide more information than in other cases. In the mass degenerate limit, however, both $S^{DQ}_{4/3}$ and $S^{DQ}_{2/3}$ contribute to the number of events in the same peak. In this case, x_{CA} depends on the relative ratio of coupling of the two diquarks to fermions. Fig. (12) shows x_{CA} for this case, $S^{DQ}_{4/3} + S^{DQ}_{4/3}$ in the limit where the diquark couplings to fermions are equal. For arbitrary ratios of couplings (but degenerate

[8] We note again that the classical case of LR symmetry has the same x_{CA} as shown here for S_{+1}.

masses) x_{CA} can vary between the two extreme limits shown as $S^{DQ}_{4/3}$ and $S^{DQ}_{2/3}$. Measurement of x_{CA} anywhere between those two extremes, therefore points toward decomposition 3-i in case of DQs. The problematic case for distinguishing between 3-i and decomposition 1-i is therefore the mass degenerate case for decomposition 3-i, where the two pairs of diquark couplings conspire to give a x_{CA} equal (or very similar) to the corresponding one for S_{+1}.

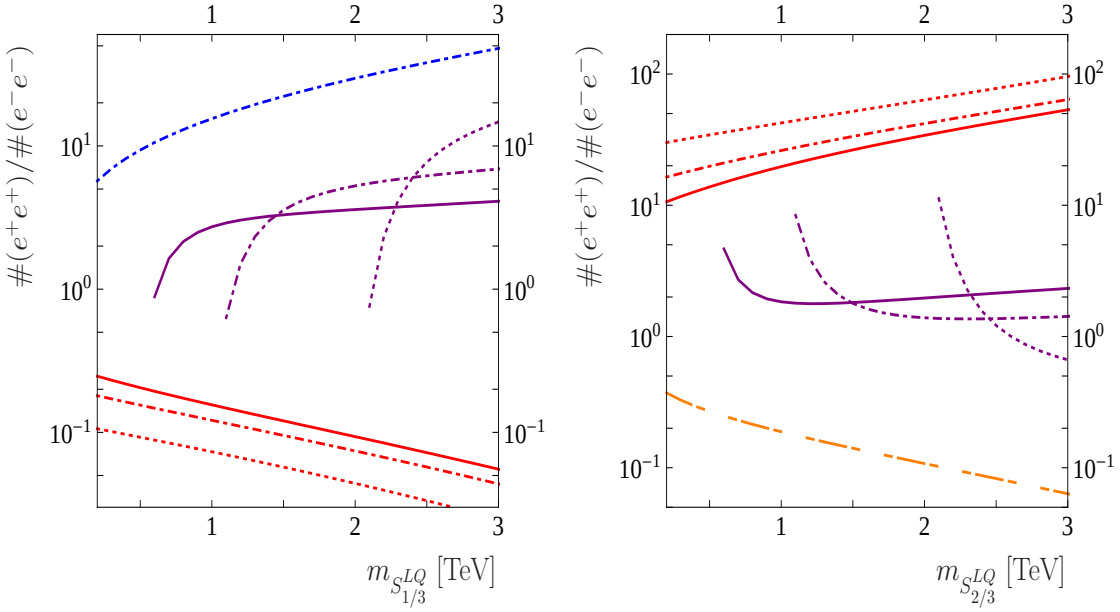

FIG. 13: Charge asymmetry x_{CA} as a function of the leptoquark mass, to the left $S^{LQ}_{1/3}$, to the right $S^{LQ}_{2/3}$. The different lines show different cases: blue (left, dash-dotted) and orange (right, dash-dotted) show x_{CA} for $S^{LQ}_{1/3}+e$ and $S^{LQ}_{2/3}+e$ production, respectively. The red lines in both plots show x_{CA} for $S^{LQ}_{q}+\psi$ production only. The purple lines show in both cases x_{CA} combining both production modes, assuming the couplings are equal, $g_{eQS^{LQ}_q} = g_{\psi Q' S^{LQ}_q}$. Shown are three calculations for different values of m_ψ: $m_\psi = 0.5$ TeV - full lines; $m_\psi = 1$ TeV - dot-dashed lines and $m_\psi = 2$ TeV - dotted lines. In all cases the calculation includes a phase space suppression for $\mathrm{Br}(S^{LQ}_{Q} \to q+\psi)$ as described in the text.

We now turn to the discussion of x_{CA} for the four decompositions with two LQs. As mentioned previously, the final states for LQs are e^-e^-jjj and e^+e^+jjj. LNV with LQs can therefore, in principle, be distinguished from DQs and S_{+1}. However, in the discussion of x_{CA} for LQs one more complication arises: The final LNV states can be produced via two different intermediate states, i.e. $S^{LQ}_q + e$ and $S^{LQ}_q + \psi$. In case of $S^{LQ}_{2/3}$, for example, the main production diagram is $d+g \to S^{LQ}_q + e^-$, contributing to e^-e^-, while $u+g \to S^{LQ}_{2/3} + \psi$ will contribute to e^+e^+-like events. For the case of $\sigma(pp \to S^{LQ}_q + \psi)$, the cross section not only depends strongly on $m_{S^{LQ}_q}$, but also depends on m_ψ, see fig. (6). However, also in the case of $S^{LQ}_q + e$ production, the mass of ψ enters in the calculation of the total number of events, since the branching ratio of $\mathrm{Br}(S^{LQ}_q \to \psi + z)$, where z stands for all possible SM

fermion states, suffers a phase space suppression factor for large m_ψ:

$$f(m_S^2, m_\psi^2) = \frac{(m_S^2 - m_\psi^2)^2}{m_S^4}. \tag{12}$$

The predicted charge asymmetry then depends on whether events from $\sigma(pp \to S_q^{LQ} + \psi)$ can be separated from $\sigma(pp \to S_q^{LQ} + e)$ or not. This separation can be done, in principle, by looking at the invariant mass peaks discussed in the next section. However, especially in case the total number of events is low, such a separation will become difficult (and inefficient). Then the charge asymmmetry measured will be an averaged charged asymmetry of both production modes.

In fig. (13) we plot calculated x_{CA} as a function of the leptoquark mass, to the left $S_{1/3}^{LQ}$, to the right $S_{2/3}^{LQ}$ for a number of cases. The blue (left, dash-dotted) and orange (right, dash-dotted) lines show x_{CA} for $S_{1/3}^{LQ} + e$ and $S_{2/3}^{LQ} + e$ production, respectively. The red lines in both plots show x_{CA} for $S_q^{LQ} + \psi$ production only. Shown are three calculations for different values of m_ψ: $m_\psi = 0.5$ TeV - full lines; $m_\psi = 1$ TeV - dot-dashed lines and $m_\psi = 2$ TeV - dotted lines. These lines are the predicted x_{CA} for the case that events from $S_q^{LQ} + \psi$ can be separated completely from those stemming from $S_{1/3}^{LQ} + e$. In the more conservative case that averaging over both production modes has to be done, the predicted x_{CA}'s are plotted as purple lines, again for three different values of m_ψ. In this calculation we assumed for simplicity that $g_{eQS_q^{LQ}} = g_{\psi Q' S_q^{LQ}}$ and included a phase space suppression factor in the calculation of events for $S_{1/3}^{LQ} + e$ production to account for the reduced $\mathrm{Br}(S_q^{LQ} \to \psi + z)$. This phase space suppression, see eq. (12), is responsible for the sharp bend in the lines at low $m_{S_q^{LQ}}$. For larger or smaller ratios of $g_{eQS_q^{LQ}}$ to $g_{\psi Q' S_q^{LQ}}$ the corresponding lines for x_{CA} will change, thus x_{CA} can vary in principle between the extremes shown in fig. (13) for arbitrary values of the couplings. However, if $m_{S_q^{LQ}}$ and m_ψ are known from measurement, the ratio of $g_{\psi Q' S_q^{LQ}}$ and $g_{eQS_q^{LQ}}$ can in principle be fixed from a measurement of $\mathrm{Br}(S_q^{LQ} \to \psi + z)$.

The above discussed results cover the decompositions 4-i and 5-i, in which the two LQs in the diagram have the same quantum numbers. For the case of decompositions 2-iii, on the other hand, both types of LQs contribute and the resulting x_{CA} will be the average of the individual x_{CA}'s shown in fig. (13) on the left and right. For all couplings equal, the resulting x_{CA} varies smoothly from around $x_{CA} = 2$ for $m_{S_q^{LQ}} = 1$ TeV to $x_{CA} \simeq 3$ for $m_{S_q^{LQ}} = 3$ TeV, for decomposition 2-iii-a. There is, however, one subtle difference between decomposition 2-iii-a and 2-iii-b, since in these two the up and down quarks in the initial state for the case of $\sigma(pp \to S_q^{LQ} + \psi)$ production is interchanged. This leads to slightly lower values for x_{CA} in 2-iii-b compared to 2-iii-a.

Finally, we briefly discuss the remaining eight decompositions within group-(3). In this case, in principle, mass peaks should show up in m^2_{eejj} and $m^2_{e_2jjj}$, clearly identifying the LQ and the other scalar boson by the individual x_{CA}'s. However, this statement assumes that cross sections for LQs are large enough that for these decompositions both types of scalars are produced at the LHC. Considering the large ratio of cross sections for S_{+1} and

DQs relative to cross sections for LQs, this might be a too optimistic assumption. Thus, in the case only one peak in m^2_{eejj} is found, only the "leading" boson of the decomposition can be identified and there appears a degeneracy among the decompositions in group-(1) and group-(3) in this observable.

B. Invariant mass peaks

We now turn to the discussion of differentiating between different decompositions using peaks in the cross sections in different experimentally measurable invariant mass systems. Again, we will divide this discussion into different cases. First, we will discuss decompositions with at least one S_{+1}, then decompositions with at least one diquark. These two cases can be distinguished, in principle, by measuring the charge asymmetry discussed in the last subsection. Finally, we will discuss decompositions which contain only LQs.

Case	m_S	m_ψ	$m_{S'}$	Decomposition
A	$m(eejj)$	$m(ejj)$	$m(jj)$	$(\bar{u}d)(\bar{e})(\bar{e})(\bar{u}d)$
B	$m(eejj)$	$m(ejj)$	$m(ej)$	$(\bar{u}d)(\bar{e})(\bar{u})(d\bar{e})$; $(\bar{u}d)(\bar{e})(d)(\bar{u}\bar{e})$
C	$m(eejj)$	$m(eej)$	$m(ee)$	$(\bar{u}d)(\bar{u})(d)(\bar{e}\bar{e})$; $(\bar{u}d)(d)(\bar{u})(\bar{e}\bar{e})$
D	$m(eejj)$	$m(eej)$	$m(ej)$	$(\bar{u}d)(\bar{u})(\bar{e})(d\bar{e})$; $(\bar{u}d)(d)(\bar{e})(\bar{u}\bar{e})$

TABLE III: *Combinations of invariant mass distributions where peaks in the cross sections arise, in case the mass ordering is $m_S > m_\psi > m_{S'}$, for decompositions of $0\nu\beta\beta$ decay with charge asymmetries that are " $(\bar{u}d)$ like". If $m_\psi \leq m_{S'}$, $m_{S'}$ can not be measured and cases A=B and C=D can not be distinguished by this observable.*

Table III shows the results of the analysis for decompositions involving S_{+1}. With the exception of case (A), where S_{+1} appears twice in the diagram, the two scalars in the decomposition are different particles. In case $m_S > m_\psi > m_{S'}$, there are then two subsystems in the sample of $eejj$-events which form mass peaks and we can distinguish cases (A)-(D), leaving only "degeneracies" in decompositions (1-ii-a)-(1-ii-b) (corresponding to case B) and (2-iii-a)-(2-iii-b) (case C), where both mass peaks and x_{CA} are (pairwise) identical. However, it is possible that $m_\psi \leq m_{S'}$, in which case $m_{S'}$ can not be measured and cases A=B and C=D can not be distinguished anymore.

Table IV shows the results of the analysis for decompositions involving DQs. Case (A) has the same invariant mass peaks as case (A) in table III. Thus, in case $m_{S^{DQ}_{4/3}} = m_{S^{DQ}_{2/3}}$ the decomposition (3-i) can not be distinguished from (1-i), if also the diquark couplings "conspire" such that x_{CA} agrees with the corresponding value for S_{+1}. In this case, the only difference between (3-i) and (1-i) is that (3-i) always requires a electrically charged coloured fermion, which could show up in pair production. Cases (B)-(D) in table IV are also equal

Case	m_S	m_ψ	$m_{S'}$	Decomposition
A	$m(eejj)$	$m(ejj)$	$m(jj)$	$(\bar{u}\bar{u})(\bar{e})(\bar{e})(dd)$
B	$m(eejj)$	$m(ejj)$	$m(ej)$	$(\bar{u}\bar{u})(\bar{e})(d)(d\bar{e})$; $(dd)(\bar{e})(\bar{u})(\bar{u}\bar{e})$
C	$m(eejj)$	$m(eej)$	$m(ee)$	$(\bar{u}\bar{u})(d)(d)(\bar{e}\bar{e})$; $(dd)(\bar{u})(\bar{u})(\bar{e}\bar{e})$
D	$m(eejj)$	$m(eej)$	$m(ej)$	$(\bar{u}\bar{u})(d)(\bar{e})(d\bar{e})$; $(dd)(\bar{u})(\bar{e})(\bar{u}\bar{e})$

TABLE IV: *As above, for decompositions of $0\nu\beta\beta$ decay with charge asymmetries that are "$(\bar{u}\bar{u})$ and (dd) like". If $m_\psi \leq m_{S'}$, $m_{S'}$ cannot be measured and cases A=B and C=D can not be distinguished with this observable.*

to (B)-(D) in table III. However, in these cases DQ decompositions and S_{+1} decompositions can always be distinguished by measuring x_{CA}.

Case	m_S	m_ψ	$m_{S'}$	Decomposition
A	$m(e_2jjj)$	$m(e_2jj)$	$m(jj)$	$(\bar{u}\bar{e})(d)(\bar{e})(\bar{u}d)$; $(\bar{u}\bar{e})(\bar{u})(\bar{e})(dd)$; $(d\bar{e})(\bar{u})(\bar{e})(\bar{u}d)$; $(d\bar{e})(d)(\bar{e})(\bar{u}\bar{u})$
B	$m(e_2jjj)$	$m(e_2jj)$	$m(e_2j)$	$(\bar{u}\bar{e})(d)(\bar{u})(d\bar{e})$; $(\bar{u}\bar{e})(d)(d)(\bar{u}\bar{e})$; $(d\bar{e})(\bar{u})(\bar{u})(d\bar{e})$; $(d\bar{e})(d)(\bar{u})(\bar{u}\bar{e})$
C	$m(e_2jjj)$	$m(jjj)$	$m(jj)$	$(\bar{u}\bar{e})(\bar{e})(\bar{u})(dd)$; $(\bar{u}\bar{e})(\bar{e})(d)(\bar{u}d)$; $(d\bar{e})(\bar{e})(\bar{u})(\bar{u}d)$; $(d\bar{e})(\bar{e})(\bar{u})(\bar{u}d)$

TABLE V: *As above, for decompositions of $0\nu\beta\beta$ decay with charge asymmetries that are "$(\bar{u}\bar{e})$ and $(d\bar{e})$ like", i.e. for single leptoquark production. Recall that the the complete signal is "eejjj" without a peak in m^2_{eejjj}. If $m_\psi \leq m_{S'}$, cases A=B cannot be distinguished. Note that case B, where both sides of the decomposition contain only leptoquarks, will produce "eejjj" final states, only. In all other cases, also the "eejj' signal should arise.*

Finally, table V shows combinations of invariant mass distributions in case the mass ordering is $m_S > m_\psi > m_{S'}$, for decompositions of $0\nu\beta\beta$ decay with charge asymmetries that are "$(\bar{u}\bar{e})$ and $(d\bar{e})$ like", i.e. for single leptoquark production. Here, it is assumed that events from $S_q^{LQ} + e$ production can be distingsuished from $S_q^{LQ} + \psi$ production. The table refers to the former. (Note again, if $m_\psi \leq m_{S'}$, cases A=B can not be distinguished, leaving a degeneracy in the identification of the decomposition in that case.) In case of events from $S_q^{LQ} + \psi$ production, the decay of the LQ will lead to a peak in $m^2_{e_a j_x} = m^2_{S_q^{LQ}}$ and the decay of ψ to $m^2_{e_b j_y j_z} = m^2_\psi$. Note, however, that in case of $S_q^{LQ} + e$ production, the mass peak for m^2_ψ is formed by a subsystem of "e_2jjj" (which gives $m^2_{S_q^{LQ}}$), whereas in $S_q^{LQ} + \psi$ production the two mass peaks must come from different leptons and jets, i.e. $a \neq b$ and $y \neq x \neq z$. This feature can be used to separate $S_q^{LQ} + e$ from $S_q^{LQ} + \psi$ production.

Before closing, we briefly mention pair production of coloured fermions. Here, a signal $eejjjj$, i.e. at least four hard jets, would test the different decompositions of double beta decay. We note that decompositions with ψ_0 exist with a colour singlet fermion, for which pair production at the LHC is negligible, while for all the 12 "new" decompositions, see discussion in section II and section III, pair production of the exotic fermions is expected to

probe the existence of such states with masses up to roughly $m_\psi \sim 2 - 2.5$ TeV, depending on the final state branching ratios. Note, that also pair produced ψ can, depending on decomposition, produce in some cases like-sign dileptons. Also, if a signal is found in $eejjjj$, there is a threshold for these events at $m_{eejjjj} = 2m_\psi$. Different subsystems again form mass peaks at m_ψ and in case, this fermion is heavier than (one of) the bosons mass peaks in sub-sub-systems will show up, providing additional information. The possible combinations can be straightforwardly derived from table I.

In summary, we have discussed two possible observables, which allow to identify which of the decompositions of table I is realized, if a positive LNV observation is made at the LHC. The combination of both observables should be sufficient to identify the correct decomposition unambigously, apart from the two pairs: (A) 1-ii-a and 1-ii-b and (B) 1-i and 3-i (the latter only in the mass degenerate case), which can lead to very similar values in both observables.

VI. SUMMARY

In this paper we have compared the discovery potential of lepton number violating signals at the LHC with the sensitivity of current and future neutrinoless double beta decay experiments, assuming that the decay rate is dominated by heavy $\mathcal{O}$ (TeV) particle exchange. We have treated the first of two possible topologies contributing to both processes which contains one fermion and two bosons in the intermediate state, and concentrated on the case where the fermion mass is always smaller than the scalar or vector masses. The topology considered corresponds to 18 possible decompositions including scalar, leptoquark and diquark mechanisms. With the exception of some leptoquark mechanisms a $0\nu\beta\beta$ decay signal corresponding to a half life in the range $10^{26} - 10^{27}$ yrs should imply a positive LNV signal at the LHC, and vice versa, the non-observation of a positive signal at the LHC would rule out a short-range mechanism for neutrinoless double beta decay in most cases. In summary the LHC search provides a complementary and in many cases even superior option to search for $\Delta L = 2$ lepton number violation for this short range case.

If $0\nu\beta\beta$ decay is triggered by light sub-eV scale Majorana neutrinos, on the other hand, its LHC analogue will be unobservable. In any case though an observation of either $0\nu\beta\beta$ decay or its analogue at the LHC will prove also the light neutrinos to be Majorana particles by virtue of the four loop contribution to the neutrino mass generation according to the Schechter-Valle thorem [56, 57]. However, this 4-loop-induced Majorana mass while bestowing the light neutrinos with Majorana-ness is too small to account for the mass squared differences observed in neutrino oscillations [58], implying that differently generated masses, either of Dirac or of Majorana type will be the dominant contributions for at least the heavier two mass eigenstates.

Moreover, we have discussed two possibilities to discriminate different contributions to the $0\nu\beta\beta$ decay rate by using LHC observables: First, the charge asymmetry corresponding to the ratio of positive like sign electron events and negative like sign electron events, which

reflects the larger abundance of u quarks compared to d quarks in the most simple cases but becomes a more complicated function of masses and couplings in the general case. For large masses of the resonantly produced particles this asymmetry can vary by up to 7 orders of magnitude. And second, the resonance peaks at the invariant mass distribution of the decay products of the heavy particles produced on-shell. The various resonance peaks depend on the mass ordering of the intermediate particles and on the exact decomposition and can then be used to identify the intermediate particles triggering the decay. Consequently, if an LNV signal at the LHC would be found it should be possible to identify the dominant contribution of $0\nu\beta\beta$ decay.

Acknowledgements

We are grateful to Alfonso Zerwekh for useful discussions. J.C.H. thanks the IFIC for hospitality during his stay. This work was supported by UNILHC PITN-GA-2009-237920 and by the Spanish MICINN grants FPA2011-22975, MULTIDARK CSD2009-00064, by the Generalitat Valenciana (Prometeo/2009/091), by Fondecyt (Chile) under grants 11121557, 1100582 and by CONICYT (Chile) project 791100017. HP was supported by DGF grant PA 803/6-1.

I. APPENDIX A. LAGRANGIANS

Here we specify the Lagrangian terms used in our analysis.

As was discussed in section II there are two possible topologies for the tree-level diagrams fig. 2 constructed of renormalizable interactions which contribute to $0\nu\beta\beta$-decay and production of like-sign dileptons in pp-collisions. It is implied that gluons could be attached to any colorful external or internal line of these diagrams. In the present paper we focus on the Topology I corresponding to fig. 2(a). All the possible particles with their SM assignments in the intermediate states of these diagrams are listed in table I taken from ref. [22]. These diagrams or their parts without the gluon insertions represent mechanisms of $0\nu\beta\beta$-decay studied in the present paper. Examples of Feynman diagrams are shown in figs. 3, 4.

For our study it is sufficient to list renormalizable operators corresponding to the vertices of these diagrams in the representation with physical mass eigenstates after the electroweak symmetry breaking. The SM gauge invariant representation in terms of the electroweak interaction eigensates can be found in Refs. [22, 40]. For the fields we adopt notations

$$F^{(n)}_{Q_{em}} \tag{A.1}$$

where n is a dimension of the $SU(3)_c$ representation to which belongs a field F and Q_{em} is its electric charge. We use $F = S$ and $F = V_\mu$ for the scalar and vector fields respectively.

Below we specify the interactions of the scalar fields S. The interactions of the vector fields can be readily derived from them by substitution $S \to S^\mu$ with the same charge and SU_{3C} assignment and by simultaneous insertion of γ_μ to the coupled fermionic current.

We start with the interactions of the scalar $S^{(1,8)}_{+1}$ fields participating in decompositions 1-i, 1-ii, and 2-i, 2-ii from table I. In our numerical analysis we use S_{+1} for $S^{(1)}_{+1}$. These

fields interact with quarks, charged leptons and fermions $\psi_0^{(1,8)}$ and $\psi_{5/3}^{(3)}, \psi_{4/3}^{(\bar{3})}$ according to the Lagrangian:

$$\begin{aligned}\mathcal{L}_{S_{+1}} &= g^{(k)X}_{udS_{+1}}\left(\bar{u}\ \hat{S}^{(k)}_{+1}P_X\ d\right) + g^{(k)X}_{e^c\psi_0 S_{+1}}\left(\overline{e^C}\ P_X\ \psi_0^{(k)}\right) S^{(k)}_{+1} + g^{(k)X}_{e\psi_0 S_{+1}}\left(\overline{e}\ P_X\ \psi_0^{(k)}\right) S^{(k)\dagger}_{+1} + \\ &+ g^X_{u\psi_{5/3}S_{+1}}\ \left(\bar{u}\ P_X\ \psi^{(3)}_{5/3}\right) S^{(1)}_{+1} + g^X_{d\psi_{4/3}S_{+1}}\ \left(\bar{d}\ P_X\ \psi^{(\bar{3})^C}_{4/3}\right) S^{(1)}_{+1} + \\ &- m^{(k)}_{\psi_0}\ \overline{\psi_0^{(k)}}\psi_0^{(k)} + \text{h.c.}.\end{aligned} \tag{A.2}$$

The indices $X = L, P$ are independent in all the terms. The generation indexes $i, j = 1, 2, 3$ of the quarks u, d and charged leptons e are suppressed. We use the shorthand notations: $g^{(k)}\hat{S}^{(k)} = g^{(1)}S^{(1)}\ \mathbf{I} + g^{(8)}S^{(8)A}\lambda^A/2$ with the identity and Gell-Mann matrices in the color space. Also $g^{(k)}\psi^{(k)}S^{(k)} = g^{(1)}\psi^{(1)}S^{(1)} + g^{(8)}\psi^{(8)A}S^{(8)A}$ and $m^{(k)}\psi^{(k)}\psi^{(k)} = m^{(1)}\psi^{(1)}\psi^{(1)} + m^{(8)}\psi^{(8)A}\psi^{(8)A}$. For the ψ_0 field we study an economical case with only one independent chiral component, so that in the 4-component notation it is represented by a Majorana field satisfying $\psi_0^C = \psi_0$. Thus, its mass m_{ψ_0} in the last term of eq. (A.2) is a $\Delta L = 2$ Majorana mass. We do not show the ordinary complex scalar mass term for S_{+1} and the Dirac ones for $\psi_{5/3}$, $\psi_{4/3}$.

The Majorana field cannot have definite lepton number, but for convenience it can be assigned to the chiral projections of ψ_0. One of the two options we choose is $L = 1$ for $P_L\psi_0$ and $L = -1$ for $P_R\psi_0$. The fields $\psi_{5/3}, \psi_{4/3}$ and S_{+1} have $L = 0$. Baryon number B conservation requires an assignment $B = 1/3$ for $\psi_{5/3}$, $B = -1/3$ for $\psi_{4/3}$ and $B = 0$ for S_{+1}, ψ_0 . As seen from eq. (A.2) there are two sources of LNV: the second interaction term with the coupling $g^L_{e^c\psi S}$ and the Majorana masses $m^{(1)}_{\psi_0}$ as well as $m^{(8)}_{\psi_0}$.

The scalar SU_{3C} singlet field S_{+2} appears in decompositions 1-ii, 3-ii and 3-iii of table I. Its interactions are given by:

$$\begin{aligned}\mathcal{L}_{S_{+2}} &= g^X_{eeS_{+2}}\left(\overline{e^C}\ P_X\ e\right) S_{+2} + g^X_{d\psi_{5/3}S_{+2}}\left(\overline{\psi^{(3)}_{5/3}}\ P_X\ d\right) S_{+2} + \\ &+ g^X_{u\psi_{4/3}S_{+2}}\left(\overline{u}\ P_X\ \psi^{(\bar{3})^C}_{4/3}\right) S_{+2} + \text{h.c.}\end{aligned} \tag{A.3}$$

Here the only LNV source is the first $\Delta L = 2$ term.

The diquarks $S^{DQ(3,\bar{6})}_{2/3}$ and $S^{DQ(\bar{3},6)}_{4/3}$ appear in decompositions 3-i, 3-ii, 3-iii, 4-ii and 5-ii of table I. These fields interact with quarks, charged leptons and fermions $\psi^{(3)}_{5/3}, \psi^{(\bar{3})}_{4/3}$ and $\psi^{(\bar{3},6)}_{1/3}$

in the following way:

$$\begin{aligned}
\mathcal{L}_{DQ} \;=\; & g^{(6)X}_{uuS^{DQ}_{4/3}}\,(\bar{u}\;P_X\;\hat{S}^{DQ}_{4/3}\;u^C) + g^{(6)X}_{ddS^{DQ}_{2/3}}\,(\overline{d^C}\;P_X\;\hat{S}^{DQ}_{2/3}\;d) + \\
& +\; g^{(3)X}_{d_id_jS^{DQ}_{2/3}}\,\epsilon^{IJK}(\overline{d^C}_{iI}\;P_X\;d_{jJ})S^{DQ(3)}_{2/3K} + \\
& +\; g^{(6)X}_{d\psi_{5/3}S^{DQ}_{4/3}}\,(\bar{d}\;P_X\;\hat{S}^{DQ}_{4/3}\;\psi^{(3)^C}_{5/3}) + g^{(6)X}_{u\psi_{4/3}S^{DQ}_{2/3}}\,(\overline{\psi^{(\bar{3})}_{4/3}}\;P_X\;\hat{S}^{DQ}_{2/3}\;u) + \\
& +\; g^{(3)X}_{u\psi_{4/3}S^{DQ}_{2/3}}\,\epsilon^{IJK}(\overline{\psi^{(\bar{3})}_{4/3I}}\;P_X\;u_J)S^{DQ(3)}_{2/3K} + \\
& +\; g^{X}_{e\psi_{1/3}S^{DQ}_{4/3}}\,(\overline{\psi^{(6)a}_{1/3}}\;P_X\;e)\;S^{DQ(6)}_{4/3a} + g^{(6)X}_{e\psi_{1/3}S^{DQ}_{2/3}}\,(\overline{e^C}\;P_X\;\psi^{(6)}_{1/3a})\;S^{DQ(\bar{6})a}_{2/3} + \\
& +\; g^{(3)X}_{e\psi_{1/3}S^{DQ}_{2/3}}\,(\overline{e^C}\;P_X\;\psi^{(\bar{3})I}_{1/3})\;S^{DQ(3)}_{2/3\;I}\;.
\end{aligned} \tag{A.4}$$

Here $I, J, K = 1-3$ and $a = 1-6$ are the color triplet and sextet indexes respectively. As before the generation indexes $i, j = 1, 2, 3$ of the quarks u, d and charged leptons e are suppressed in all the terms except for the third one which vanishes if $i = j$. For convenience we introduced notations $\hat{S}^{DQ}_{4/3} = S^{DQ(6)}_{4/3a}(T_{\bar{\mathbf{6}}})^a_{IJ}$ and $\hat{S}^{DQ}_{2/3} = S^{DQ(\bar{6})a}_{2/3}(T_{\mathbf{6}})^{IJ}_a$. In the terms with these matrix fields summation over the triplet indexes I, J is implied. The symmetric 3×3 matrices $T_{\mathbf{6}}$ and $T_{\bar{\mathbf{6}}}$ can be found in ref. [22]. As seen from eq. (A.4) the sources of LNV in the diquark interactions in are given by the last two $\Delta L = 2$ terms with $\psi_{1/3}$ fields. We assign to $\psi^{(\bar{3},6)}_{1/3}$ a lepton number $L = 1$.

The leptoquark SU_{3C} 3-plet fields $S^{LQ}_{2/3}$ and $S^{LQ}_{-1/3}$ participate in decompositions 2, 4 and 5 of table I. Their interactions we write in the form:

$$\begin{aligned}
\mathcal{L}_{LQ} \;=\; & g^{X}_{euS^{LQ}_{-1/3}}\,(\bar{u}^I\;P_X\;e^C)\;S^{LQ}_{-1/3\;I} + g^{X}_{edS^{LQ}_{2/3}}\,(\bar{d}^I\;P_X\;e)\;S^{LQ}_{2/3\;I} \\
& +\; g^{(1)X}_{u\psi_0S^{LQ}_{2/3}}\,(\bar{u}^I\;P_X\;\psi^{(1)}_0)\;S^{LQ}_{2/3\;I} + g^{(8)X}_{u\psi_0S^{LQ}_{2/3}}\,(\bar{u}\;P_X\;\hat{\psi}_0)\;S^{LQ}_{2/3} + \\
& +\; g^{(1)X}_{d\psi_0S^{LQ}_{-1/3}}\,(\bar{d}\;P_X\;\hat{\psi}_0)\;S^{LQ}_{-1/3} + g^{(8)X}_{d\psi_0S^{LQ}_{-1/3}}\,(\bar{d}\;P_X\;\hat{\psi}_0)\;S^{LQ}_{-1/3} + \\
& +\; g^{(3)X}_{d\psi_{1/3}S^{LQ}_{2/3}}\,\epsilon_{IJK}(\bar{d}^I\;P_X\;\psi^{(\bar{3})J}_{1/3})\;S^{LQ,K^\dagger}_{2/3} + g^{(6)X}_{d\psi_{1/3}S^{LQ}_{2/3}}\,(\bar{d}\;P_X\;\hat{\psi}_{1/3})\;S^{LQ^\dagger}_{2/3} \\
& +\; g^{(3)X}_{u\psi_{1/3}S^{LQ}_{-1/3}}\,\epsilon_{IJK}(\bar{u}^I\;P_X\;\psi^{(\bar{3})J}_{1/3})\;S^{LQ,K^\dagger}_{-1/3} + g^{(6)X}_{u\psi_{1/3}S^{LQ}_{-1/3}}\,(\bar{u}\;P_X\;\hat{\psi}_{1/3})\;S^{LQ^\dagger}_{-1/3} \\
& +\; g^{X}_{e\psi_{4/3}S^{LQ}_{-1/3}}\,(\overline{e^C}\;P_X\;\psi^{(\bar{3})I}_{4/3})\;S^{LQ}_{-1/3\;I} + g^{X}_{e\psi_{5/3}S^{LQ}_{2/3}}\,(\overline{e^C}\;P_X\;\psi^{(3)}_{5/3\;I})\;S^{LQ,I^\dagger}_{2/3}\;.
\end{aligned} \tag{A.5}$$

As before we introduce a short-hand notation $\hat{\psi}_{1/3} = \psi^{(6)}_{1/3\;a}(T_{\bar{\mathbf{6}}})^a_{IJ}$. Here $I, J = 1, 2, 3$ are the color triplet indexes. We adopt the following assignment of lepton L and baryon numbers to the leptoquarks: $L = 1,\ B = 1/3$ for $S^{LQ}_{-1/3}$ and $L = -1,\ B = 1/3$ for $S^{LQ}_{2/3}$. Checking the total lepton number of each term in eq. (A.5) one finds that the terms in the 2nd line with chirality $X = R$, in the 3rd line with $X = L$, in the 4th and the last lines with any X break lepton number in two units.

The following comments on the structure of the $\Delta L = 2$ amplitude is in order. For the analysis of $0\nu\beta\beta$-decay we introduced in eq. (5) an effective masses M_{eff} and an effective

couplings g_{eff}. The quantities M_{eff}^5 and g_{eff}^4 represent respectively the products of the particle masses originating from their propagators and the products of four couplings, g_i, of those operators from eqs. (A.2)-(A.5) which participate in the decomposition in question. Let us specify possible characteristic cases for combinations of these masses and couplings in $0\nu\beta\beta$ amplitude. Schematically one can distinguish the following cases:

$$\begin{aligned}\mathcal{A}(0\nu\beta\beta) &\sim g_1 g^X_{2\psi_0} g^X_{3\psi_0} g_4 \frac{m_{\psi_0}}{m^2_{S_1} m^2_{S_2} m^2_{\psi_0}} \ , \\ &\sim \not{g}_1 g^X_{2\psi_Q} g^X_{3\psi_Q} g_4 \frac{m_{\psi_Q}}{m^2_{S_1} m^2_{S_2} m^2_{\psi_Q}} \ , \quad \not{g}_1 g^L_{2\psi} g^R_{3\psi} g_4 \frac{\langle \gamma_\mu q^\mu \rangle}{m^2_{S_1} m^2_{S_2} m^2_{\psi}} \ , \\ &\sim g_1 \not{g}^X_{2\psi_0} \not{g}^X_{3\psi_0} g_4 \frac{m_{\psi_0}}{m^2_{S_1} m^2_{S_2} m^2_{\psi_0}} .\end{aligned} \tag{A.6}$$

Here, $X = L, R$ and $g_{i\psi}$ are the couplings of the operators involving ψ-field. These fields with nonzero charge Q are denoted as ψ_Q. Without this index they can be both charged ψ_Q and neutral ψ_0. The masses m_{ψ_Q} of the ψ_Q fields are of Dirac $\Delta L = 0$ type while in the case of the ψ_0 fields their masses m_{ψ_0} are of Mjorana $\Delta L = 2$ type. By $\not{g}_i$ we denote the coupling of the $\Delta L = 2$ operators. In the case of only one slash, as in the second line, it may take place in any of the four couplings, while the two slashed couplings can only be of the $\not{g}_{i\psi_0}$-type as in the last line. In the combination given in the first line the $\Delta L = 2$ is brought by the Majorana mass m_{ψ_0} while in both cases of the second line it is due to a single $\not{g}_i$ coupling. The combination of the last line put together three sources of the $\Delta L = 2$ in a total $\Delta L = 2$. Note that the expressions in eq. (A.6) imply that the masses of the intermediate particles $m_i \gg |\mathbf{q}|$ where $\mathbf{q}$ are their momenta whose mean value is about ~ 100 MeV. The numerator of the third combination $\langle \gamma_\mu q^\mu \rangle$ implies inception of γ_μ in between of the two electron or two quark bispinors depending on the considered decomposition. It is of the order of $\mathbf{q} \sim 100$ MeV and, therefore, the third term corresponding to the LR chirality structure is suppressed in comparison with the remaining LL or RR terms by a factor of $\mathbf{q}/m_\psi$. Thus, among all the possible cases specified in (A.6) survive only those with LL or RR chiralities leading to

$$\mathcal{A}(0\nu\beta\beta) \sim \frac{g_{eff}^4}{M_{eff}^5} \tag{A.7}$$

in terms of the effective quantities introduced in eq. (5). The decompositions leading to the third term in eq. (A.6) are very weakly constrained by $0\nu\beta\beta$ decay experiments. However they can be probed at the LHC in the way we discussed in the main text.

[1] R. N. Mohapatra and G. Senjanovic, Phys.Rev. **D23**, 165 (1981).

[2] M. Doi, T. Kotani, and E. Takasugi, Prog.Theor.Phys.Suppl. **83**, 1 (1985).

[3] R. Mohapatra, Phys.Rev. **D34**, 3457 (1986).

[4] M. Hirsch, H. Klapdor-Kleingrothaus, and S. Kovalenko, Phys.Rev.Lett. **75**, 17 (1995).

[5] A. Faessler, S. Kovalenko, and F. Simkovic, Phys.Rev. **D58**, 055004 (1998), arXiv:hep-ph/9712535.
[6] M. Hirsch and J. Valle, Nucl.Phys. **B557**, 60 (1999), arXiv:hep-ph/9812463.
[7] M. Hirsch, H. Klapdor-Kleingrothaus, and S. Kovalenko, Phys.Rev. **D54**, 4207 (1996), arXiv:hep-ph/9603213.
[8] P. Bamert, C. Burgess, and R. Mohapatra, Nucl.Phys. **B438**, 3 (1995), arXiv:hep-ph/9408367.
[9] P. Benes, A. Faessler, F. Simkovic, and S. Kovalenko, Phys.Rev. **D71**, 077901 (2005), arXiv:hep-ph/0501295.
[10] O. Panella and Y. N. Srivastava, Phys.Rev. **D52**, 5308 (1995), arXiv:hep-ph/9411224.
[11] G. Bhattacharyya, H. Klapdor-Kleingrothaus, H. Pas, and A. Pilaftsis, Phys.Rev. **D67**, 113001 (2003), arXiv:hep-ph/0212169.
[12] S. Choubey, M. Duerr, M. Mitra, and W. Rodejohann, JHEP **1205**, 017 (2012), arXiv:1201.3031.
[13] B. Brahmachari and E. Ma, Phys.Lett. **B536**, 259 (2002), arXiv:hep-ph/0202262.
[14] P.-H. Gu, Phys.Rev. **D85**, 093016 (2012), arXiv:1101.5106.
[15] M. Kohda, H. Sugiyama, and K. Tsumura, (2012), arXiv:1210.5622.
[16] F. F. Deppisch, M. Hirsch, and H. Pas, (2012), arXiv:1208.0727.
[17] SuperNEMO Collaboration, R. Arnold et al., Eur.Phys.J. **C70**, 927 (2010), arXiv:1005.1241.
[18] M. Hirsch, K. Muto, T. Oda, and H. Klapdor-Kleingrothaus, Z.Phys. **A347**, 151 (1994).
[19] F. Deppisch and H. Pas, Phys.Rev.Lett. **98**, 232501 (2007), arXiv:hep-ph/0612165.
[20] H. Pas, M. Hirsch, H. Klapdor-Kleingrothaus, and S. Kovalenko, Phys.Lett. **B453**, 194 (1999).
[21] H. Pas, M. Hirsch, H. Klapdor-Kleingrothaus, and S. Kovalenko, Phys.Lett. **B498**, 35 (2001), arXiv:hep-ph/0008182.
[22] F. Bonnet, M. Hirsch, T. Ota, and W. Winter, JHEP **1303**, 055 (2013), arXiv:1212.3045.
[23] H. Klapdor-Kleingrothaus et al., Eur.Phys.J. **A12**, 147 (2001), arXiv:hep-ph/0103062.
[24] EXO Collaboration, M. Auger et al., Phys.Rev.Lett. **109**, 032505 (2012), arXiv:1205.5608.
[25] KamLAND-Zen Collaboration, A. Gando et al., Phys. Rev. Lett. **110**, 062502 (2013), arXiv:1211.3863.
[26] ATLAS Collaboration, G. Aad et al., Eur.Phys.J. **C72**, 2056 (2012), arXiv:1203.5420.
[27] CMS Collaboration, (2012), PAS EXO-12-017.
[28] W.-Y. Keung and G. Senjanovic, Phys.Rev.Lett. **50**, 1427 (1983).
[29] A. Ferrari et al., Phys.Rev. **D62**, 013001 (2000).
[30] S. Gninenko, M. Kirsanov, N. Krasnikov, and V. Matveev, Phys.Atom.Nucl. **70**, 441 (2007).
[31] V. Bansal, (2009), arXiv:0910.2215.
[32] M. Hirsch, H. Klapdor-Kleingrothaus, and O. Panella, Phys.Lett. **B374**, 7 (1996), arXiv:hep-ph/9602306.
[33] H. K. Dreiner, P. Richardson, and M. H. Seymour, Phys.Rev. **D63**, 055008 (2001), arXiv:hep-ph/0007228.
[34] B. Allanach, C. Kom, and H. Pas, Phys.Rev.Lett. **103**, 091801 (2009), arXiv:0902.4697.
[35] B. Allanach, C. Kom, and H. Pas, JHEP **0910**, 026 (2009), arXiv:0903.0347.

[36] S. Kovalenko, Z. Lu, and I. Schmidt, Phys.Rev. **D80**, 073014 (2009), arXiv:0907.2533.
[37] I. de Medeiros Varzielas et al., (2012), arXiv:1210.6239.
[38] J. Helo, M. Hirsch, S. Kovalenko, and H. Pas, (2013), arXiv:1303.0899.
[39] J. C. Helo, M. Hirsch, S. Kovalenko, and H. Päs, (2013), arXiv:13xx.yyyy.
[40] T. Han, I. Lewis, and Z. Liu, JHEP **1012**, 085 (2010), arXiv:1010.4309.
[41] A. Faessler, V. Rodin, and F. Simkovic, J.Phys. **G39**, 124006 (2012), arXiv:1206.0464.
[42] A. Pukhov, (2004), arXiv:hep-ph/0412191.
[43] J. Alwall, M. Herquet, F. Maltoni, O. Mattelaer, and T. Stelzer, JHEP **1106**, 128 (2011), arXiv:1106.0522.
[44] J. C. Pati and A. Salam, Phys.Rev. **D10**, 275 (1974).
[45] R. Mohapatra and J. C. Pati, Phys.Rev. **D11**, 2558 (1975).
[46] GERDA Collaboration, I. Abt et al., (2004), arXiv:hep-ex/0404039.
[47] GERDA Collaboration, K.-H. Ackermann et al., (2012), arXiv:1212.4067.
[48] F. Alessandria et al., (2011), arXiv:1109.0494.
[49] KamLAND-Zen Collaboration, A. Gando et al., Phys.Rev. **C85**, 045504 (2012), arXiv:1201.4664.
[50] EXO-200 Collaboration, D. Auty, Recontres de Moriond, http://moriond.in2p3.fr/ (2013).
[51] Majorana Collaboration, C. Aalseth et al., Nucl.Phys.Proc.Suppl. **217**, 44 (2011), arXiv:1101.0119.
[52] A. Barabash, (2012), arXiv:1209.4241.
[53] A. Belyaev, C. Leroy, R. Mehdiyev, and A. Pukhov, JHEP **0509**, 005 (2005), arXiv:hep-ph/0502067.
[54] J. Cieza Montalvo, O. J. Eboli, M. Magro, and P. Mercadante, Phys.Rev. **D58**, 095001 (1998), arXiv:hep-ph/9805472.
[55] G. Durieux, J.-M. Gerard, F. Maltoni, and C. Smith, Phys.Lett. **B721**, 82 (2013), arXiv:1210.6598.
[56] J. Schechter and J. Valle, Phys.Rev. **D25**, 2951 (1982).
[57] M. Hirsch, S. Kovalenko, and I. Schmidt, Phys.Lett. **B642**, 106 (2006), arXiv:hep-ph/0608207.
[58] M. Duerr, M. Lindner, and A. Merle, JHEP **1106**, 091 (2011), arXiv:1105.0901.